R. & M. No. 3694

MINISTRY OF DEFENCE
(PROCUREMENT EXECUTIVE)

AERONAUTICAL RESEARCH COUNCIL
REPORTS AND MEMORANDA

Calculations of the Flow over Thick, Conical, Slender Wings with Leading-Edge Separation

By J. H. B. SMITH

LONDON: HER MAJESTY'S STATIONERY OFFICE
1972

PRICE £2·40 NET

Calculations of the Flow over Thick, Conical, Slender Wings with Leading-Edge Separation

By J. H. B. SMITH

Reports and Memoranda No. 3694*
March, 1971

Summary.

The vortex-sheet model of leading-edge separation previously applied to flat-plate delta wings has been applied to thick delta wings in the form of rhombic cones. The simplifications introduced by the use of slender-body theory and an asymptotic treatment for the core of the vortex have been retained. The results show that the vortex sheet leaves the wing tangentially to the lower surface. The calculations reproduce the observed trends with increasing thickness: the vortex core moves upwards and outwards and the circulation and both the linear and non-linear parts of the lift fall off. The quantitative agreement between theory and experiment worsens somewhat as the thickness increases, probably indicating an increase in the influence of the secondary separation.

*Replaces RAE Technical Report 71057—A.R.C.33 024.

LIST OF CONTENTS

1. *Introduction.*

The phenomena of leading-edge separation from wings of low aspect ratio have frequently been described. A number of theoretical models have been developed to treat the flows which result. The phenomena and the earlier methods have been reviewed by the author[1]. Subsequently, Polhamus[2] has published a successful heuristic correlation between the non-linear lift produced and the leading-edge suction predicted by the theory of attached flow. Ermolenko[3] has calculated the flow past a rectangular wing of low aspect ratio, assuming a form for the vortex sheets from the side edges, and Belotserkovskii[4] has further advanced the treatment of side edge separations. Nangia and Hancock[5] have applied the single-vortex model, as used by Brown and Michael[6], to delta wings in subsonic flow. Of these contributions to the problem of leading-edge separation, Refs. 2 and 5 both allow, explicitly or implicitly, for the upstream influence of the trailing edge and are therefore applicable to the calculation of overall forces in subsonic flow, unlike slender-body theory methods such as that of Ref. 1, which are only valid well upstream of subsonic trailing edges. However, as with the methods of Gersten[7] and Garner and Lehrian[8] the flow model has to be simplified to permit this.

Other recent work, by Sacks, Lundberg and Hanson[9] and by Levinski *et al.*[10,11], retains the slender-body approximation, at least for the non-linear lift. Ref. 9 deals with non-conical thin wings, mounted symmetrically on bodies of revolution, by tracing the paths of discrete vortices shed from points along the leading edge. The consequent rolling-up process is naturally irregular, but the overall force and moment are not very sensitive to this if enough vortices are introduced. The shedding rate at the leading edge can be determined either by applying the Kutta-Joukowski condition there or else on an empirical basis. Levinski and Wei[10] extend the author's method[1] to deal with combinations of thin delta wings and conical bodies of circular or elliptic cross-section. Levinski, Wei and Maki[11] treat non-conical combinations of thin wings and bodies with circular or elliptic sections, using the vortex-sheet model of Ref. 1 and the body representation of Ref. 10. They write the boundary conditions as ordinary differential equations with the streamwise distance as the independent variable, as in Ref. 12. Finally, there have been two further applications of the single-vortex model: Jobe[13] has treated cambered wings and Portnoy and Russell[14] have treated conical wings with small, but non-zero, thickness.

So far no calculations have appeared involving the formation of a vortex sheet from an edge at which the upper and lower surfaces meet at a non-zero angle. Maskell's similarity theory[15,16] draws attention to the importance of edge angle in determining the development of the vortex, edge angle being one of the parameters of the similarity relations. Rott[17] has conjectured that difficulties would arise in calculating a vortex-sheet model for separation from a wedge of non-zero angle. Delta wings in the form of cones with rhombic cross-sections have been studied in a wide range of experiments. At low wind speeds, Kirkpatrick has measured the normal force[18] on the forward part of models, where the flow is almost conical, the position of the core of the vortex[19] and the circulation about the vortex[20]. Russell[14] has measured surface pressure distributions and surveyed flow fields, also at low speeds. Pressure distributions have been measured by Britton[21] at supersonic speeds and by Smith and Kurn[22] at subsonic and transonic speeds. Wyatt and East[23] have measured skin friction and pressure distributions at low speeds.

The present paper presents calculations made by the method of Ref. 1 for the flow past wings in the form of rhombic cones with flow separation from the leading edge. The method involves the representation of the circulation in the vortices in the real viscous flow by spiral vortex sheets arising from the leading edges in an inviscid, potential-flow model. The position and strength of these sheets are determined by the conditions that they form stream surfaces with no jump in pressure across them. The inner parts of the spiral sheets are replaced by isolated vortices, on the basis of asymptotic solutions. This model is then treated by slender-body theory.

The numerical treatment uses the simplest finite difference representations and finds vortex-sheet shapes and strengths, and isolated vortex positions and strengths, which satisfy the boundary conditions, by using three iterative procedures. One of these, that which determines the vortex position, was a source of difficulty in the solutions for a flat wing, so a modified procedure has been devised. Levinski and Wei[10] use a third, apparently very satisfactory, procedure. The only other change from Ref. 1 arises from the change in wing shape. The use of slender-body theory reduces the problem to the solution of Laplace's

equation in the cross-flow plane and the first step is the conformal transformation of the cross-section of the wing. Since this is now a rhombus, a Schwarz-Christoffel transformation is needed instead of the simple Joukowski transformation used previously. The boundary condition on the wing is satisfied by a distribution of sources on the transformed contour.

Starting approximations for the iterations are readily available from the previous solutions for flat plates. Solutions have been found for wings of gradually increasing thickness at constant incidence and then further solutions found for wings of typical, fixed thickness through ranges of incidence. In this way, the same combination of incidence and thickness is arrived at along different paths in the incidence-thickness plane. When this happens, the solutions are found to be very close. For the flat plate, the tangent to the vortex sheet at the leading edge lies in the wing plane and is therefore symmetrically placed with respect to the upper and lower surfaces. As the thickness increases, the solutions which emerge from the iterative procedure show that the sheet remains tangential to the lower surface of the wing. No difficulty was encountered in calculating the solution near the leading edge.

The calculated solutions show variations of normal force, vortex position and circulation with thickness and incidence which are very similar to those observed. However, the small discrepancies between calculation and experiment observed in Ref. 1 for flat plates become larger as the thickness increases. It is likely that this can be attributed to a growing influence of the secondary separation as the thickness increases and the primary vortex weakens. Such an increase in the role of the secondary separation was predicted by Rott[17] in an analogous problem. For the thinner wings, which are of greater practical importance, the agreement between theory and experiment is satisfactory. In particular, the theory confirms the existence of appreciable reductions in lift from the flat-plate values at small edge angles, a point which complicates comparisons between calculations for wings of vanishing thickness and measurements for thin plates with chamfered edges.

The material of this Report was given a brief interim presentation at the eighth Biennial Symposium on Fluid Mechanics at Tarda, Poland in September 1967.

2. *Formulation of the Problem.*

The mathematical model of the flow is the same as that used in Ref. 1 and the treatment of it is similar. An abbreviated presentation is therefore sufficient, keeping the same basic notation.

Fig. 1 shows the wing, the coordinate system and the vortex models. The origin O of a rectangular cartesian system is taken at the apex of the wing with Ox along the axis of the wing, Oy to starboard and Oz upwards. The undisturbed stream of speed U makes an angle α with Ox. The section of the wing by a plane $x=$ constant is a rhombus, of semi-span $s=Kx$, with an interior angle δ at the leading edge. It is convenient to introduce $\varepsilon=(\pi-\delta)/2\pi$, so that $\varepsilon\pi$ is the angle shown in Fig. 1. Then $\delta=0$, $\varepsilon=0{\cdot}5$ corresponds to the flat plate, $\delta=\pi/2$, $\varepsilon=0{\cdot}25$ corresponds to a wing of square cross-section, and when $\delta\to\pi$, $\varepsilon\to 0$ the wing disappears into the vertical plane of symmetry.

On the port half-wing is sketched the rolled-up spiral vortex sheet of indefinite extent which is taken in the first place to represent the circulation distribution of the leading-edge vortex. On the starboard half-wing is shown the approximation used for calculation purposes. All the circulation on the sheet from a line OE onwards is concentrated into a line vortex along OV. This leaves behind a cut, across which the velocity potential jumps by an amount equal to the circulation of the line vortex. This is the configuration to which we are to apply slender-body theory.

Ward's[24] development of slender-body theory uses axes related to the undisturbed stream, but the transition to the present system presents no difficulty for small angles of incidence. He finds that the velocity potential can be expressed as the sum of a function of x, which depends on the Mach number and takes different forms for subsonic, transonic and supersonic speeds, and a harmonic function of y and z. It is convenient to write the slender-body approximation to the complete potential as

$$U(x+b_0(x))+\Phi,$$

where

$$2\pi b_0(x)=S'(x)\,ln\,\beta/2+\tfrac{1}{2}\int_{\dot{x}}^{\dot{1}} S''(t)\,ln\,(t-x)dt-\tfrac{1}{2}\int_{\dot{0}}^{\dot{x}} S''(t)\,ln\,(x-t)dt\,,$$

with $\beta^2=1-M^2$, for subsonic speeds, and

$$2\pi b_0(x)=S'(x)\,ln\,B/2-\int_{\dot{0}}^{\dot{x}} S''(t)\,ln\,(x-t)dt\,,$$

with $B^2=M^2-1$, for supersonic speeds, where $S(x)$ is the cross-sectional area of the body. Then

$$\Phi_{yy}+\Phi_{zz}=0 \tag{1}$$

and

$$\frac{\Phi}{U}\sim\alpha z+\frac{S'(x)}{2\pi}\,ln\,r\,, \tag{2}$$

where $r^2=y^2+z^2$, at large distances from the wing, and $Ux+\Phi$ satisfies the boundary conditions on the wing and vortex sheets. For present purposes there is no need to consider $b_0(x)$ further.

The first boundary condition on the vortex sheet is that it is a stream surface, which means that

$$\Phi_n=-\frac{KUr}{s}\sin\varphi\,, \tag{3}$$

as in Ref. 1, where n is the inward normal and φ the angle between the tangent and radius vector as shown in Fig. 1. The second boundary condition on the vortex sheet is that there is no pressure difference across it, which means that

$$\Delta\Phi=\Delta\Phi_\sigma\left(r\cos\varphi-\frac{s}{KU}\Phi_{\sigma_m}\right), \tag{4}$$

again as in Ref. 1, where Δ is the difference operator across the sheet, σ is the arc length round the cross-section of the sheet and the suffix m denotes the mean value across the sheet. The boundary condition on the wing follows from (3), noting that $r\sin\varphi=s\cos\varepsilon\pi$ on the wing:

$$\Phi_n=-KU\cos\varepsilon\pi\,. \tag{5}$$

The Kutta-Joukowski condition of finite velocity at the leading edge, appropriate to separation there, must also be satisfied.

When the circulation from the sheet beyond E is concentrated into the line vortex at V, we may suppose that the cut which remains is of a form which satisfies (3). However, since $\Delta\Phi_\sigma=0$ and $\Delta\Phi\neq0$ on it, equation (4) cannot be satisfied. The best that can be done, following Brown and Michael[6], is to arrange that the total force on the vortex and cut is zero. The force on the cut arises from a constant pressure difference across it, since $\Delta\Phi$ is proportional to x, and so depends only on the end points E and V. The force on the vortex depends on the velocity normal to it induced by the rest of the field, in the usual way. Introducing a complex variable $Z=y+iz$ and a complex potential W, such that $\Phi=\mathscr{R}\{W\}$, we can express the condition of zero total force as

$$\lim_{Z\to Z_V}\left(\frac{dW}{dZ}-\frac{\Gamma}{2\pi i}\frac{1}{Z-Z_V}\right)=KU\;\frac{2\bar{Z}_V-\bar{Z}_E}{s}\,, \tag{6}$$

as in Ref. 1, where Γ is the circulation of the starboard isolated vortex.

Provided W is an analytic function of Z, equation (1) will be satisfied automatically. To construct such a complex potential it is convenient to introduce a conformal transformation of the region of the Z-plane to the right of the wing and the imaginary axis into the half-plane $\mathscr{R}\{\zeta\}>0$, *see* Fig. 2a. Consider the Schwarz-Christoffel transformation

$$Z=s+\int_0^{\zeta}\left(\frac{t^2}{t^2+d^2}\right)^{\varepsilon}dt\,, \tag{7}$$

in which the points A and C on the centre line of the wing transform into points $\zeta=\pm id$. The point B at the leading edge of the wing clearly transforms into the origin $\zeta=0$. We have

$$\frac{dZ}{d\zeta}=\left(\frac{\zeta^2}{\zeta^2+d^2}\right)^{\varepsilon}.$$

To complete the definition of the transformation, we write $\zeta-id=r_1e^{i\theta_1}$, $\zeta=r_2e^{i\theta_2}$, $\zeta+id=r_3e^{i\theta_3}$, as in Fig. 2a, and specify

$$\frac{dZ}{d\zeta}=\left|\frac{dZ}{d\zeta}\right|e^{i\varepsilon(2\theta_2-\theta_1-\theta_3)}.$$

Then, as $\zeta\to\infty$, $\theta_1\to\theta_2\to\theta_3$ and $dZ/d\zeta\to1$, so the neighbourhood of the point at infinity is preserved. Also we have:

$$\text{on } AD,\ \theta_1=\theta_2=\theta_3=\frac{\pi}{2} \qquad \text{and arg}\frac{dZ}{d\zeta}=0\,,$$

$$\text{on } AB,\ \theta_1=-\frac{\pi}{2},\ \theta_2=\theta_3=\frac{\pi}{2} \text{ and arg}\frac{dZ}{d\zeta}=\pi\varepsilon\,,$$

$$\text{on } BC,\ \theta_1=\theta_2=-\frac{\pi}{2},\ \theta_3=\frac{\pi}{2} \text{ and arg}\frac{dZ}{d\zeta}=-\pi\varepsilon\,,$$

$$\text{on } CD,\ \theta_1=\theta_2=\theta_3=-\frac{\pi}{2} \qquad \text{and arg}\frac{dZ}{d\zeta}=0\,.$$

The transformation therefore correctly distorts the boundary of the region and is obviously analytic within it. It is therefore the transformation required. The lengths d and s are related by considering the point A or C:

$$is\cot\varepsilon\pi=s+\int_0^{id}e^{i\varepsilon\pi}\left|\left(\frac{t^2}{t^2+d^2}\right)^{\varepsilon}\right|dt\,.$$

This can be written as

$$\frac{s}{d}=\sin\varepsilon\pi\int_0^1\left(\frac{t^2}{1-t^2}\right)^{\varepsilon}dt$$

$$= \sin \varepsilon\pi \, \Gamma(\varepsilon+\tfrac{1}{2})\Gamma(1-\varepsilon)/\pi^{\frac{1}{2}} = \tfrac{1}{2} \sin \varepsilon\pi \, B(\varepsilon+\tfrac{1}{2}, 1-\varepsilon), \tag{8}$$

using the same notation as Gradshteyn and Ryzhik[25] for the gamma and beta functions. The variation of s/d with ε is shown in Fig. 2b.

The boundary condition (5) of constant normal velocity on the wing can be satisfied by a distribution of sources on the image of the wing in the ζ-plane. The normal velocity needed in the ζ-plane is

$$KU \cos \varepsilon\pi \left| \frac{dZ}{d\zeta} \right| , \text{ directed outwards from the slit } ABC.$$

This distribution of normal velocity is produced by a distribution of sources of strength

$$2KU \cos \varepsilon\pi \left| \frac{dZ}{d\zeta} \right| \text{ per unit length on } ABC.$$

The total source strength is then

$$2KU \cos \varepsilon\pi \int_C^A \left| \frac{dZ}{d\zeta} \right| |d\zeta| = 4KU \cos \varepsilon\pi \int_B^A \frac{dZ}{d\zeta} e^{-i\pi\varepsilon} \frac{d\zeta}{i}$$

$$= -4ie^{-i\pi\varepsilon} KU \cos \varepsilon\pi (Z_A - Z_B) = 4sKU \cot \varepsilon\pi = US'(x).$$

Hence the sources produce the logarithmic behaviour of Φ at large distances which is specified by (2). The remaining term in (2) is produced, without disturbing the wing boundary condition, by a uniform stream parallel to the imaginary axis in the ζ-plane. The complex conjugate of the cross-flow velocity for the attached flow in the ζ-plane can therefore be written as

$$-i\alpha U + \frac{1}{2\pi} \int_{-id}^{id} 2KU \cos \varepsilon\pi \left| \left(\frac{t^2}{t^2+d^2} \right)^{\varepsilon} \right| \frac{1}{\zeta - t} \frac{dt}{i}. \tag{9}$$

To complete the velocity field, the same representation of the leading-edge vortices in the ζ-plane is used as in Ref. 1, i.e. an isolated vortex of strength Γ at ζ_V, a sheet extending along $\zeta = \zeta(\vartheta)$ from $\vartheta = 0$ to $\vartheta = \vartheta_{\max}$, and the images of these in the imaginary axis, as sketched in Fig. 3. Taken with (9), these produce a complex conjugate velocity

$$\frac{dW}{d\zeta} = -i\alpha U + \frac{KU \cos \varepsilon\pi}{i\pi} \int_{-id}^{id} \left| \left(\frac{t^2}{t^2+d^2} \right)^{\varepsilon} \right| \frac{dt}{\zeta - t} +$$

$$+ \frac{\Gamma}{2\pi i} \left(\frac{1}{\zeta - \zeta_V} - \frac{1}{\zeta + \bar{\zeta}_V} \right) + \frac{1}{2\pi i} \int_0^{\vartheta_{\max}} \left(-\frac{d\Delta\Phi}{d\vartheta} \right) \left(\frac{1}{\zeta - \zeta(\vartheta)} - \frac{1}{\zeta + \bar{\zeta}(\vartheta)} \right) d\vartheta. \tag{10}$$

The complex potential W defined by (10) represents a flow field with the correct behaviour on the wing and at infinity, containing a representation of the leading-edge vortices. The numbers Γ and ζ_V and the functions $d\Delta\Phi/d\vartheta$ and $\zeta(\vartheta)$ are to be determined so as to satisfy the Kutta-Joukowski condition at the

leading edge, the conditions (3) and (4) on the finite part of the sheet, $0<\vartheta<\vartheta_{max}$, and condition (6). As in Ref. 1, the Kutta-Joukowski condition is used for Γ, equation (6) for ζ_V, equation (4) for $d\Delta\Phi/d\vartheta$ and equation (3) for $\zeta(\vartheta)$. The details are given in the next section and the results are discussed in Section 4.

3. *Numerical Treatment.*

The numerical treatment follows the same lines as that of Ref. 1. The extra complication arises from the more awkward conformal transformation (7) and the more involved expression for the attached flow (9). A more efficient method is used to determine the position of the isolated vortex from the condition of zero overall force (6).

In the numerical work, the distance d has been used as the unit of length; so, in this section, appropriate factors d must be re-introduced if proper dimensional equations are required.

3.1. *Finite Difference Representation.*

The shape of the outer part of the starboard sheet is specified in the transformed (ζ) plane by the values of the polar distance, $\bar{r}$,

$$d_2, d_4, \ldots . d_{2n}$$

of a set of n pivotal points on the sheet measured from the position of the starboard isolated vortex, ζ_V, as shown in Fig. 3. The points are located at fixed, arbitrarily chosen, values of the polar angle, ϑ, measured about ζ_V from the line joining it to the origin. These values of ϑ are denoted by

$$h_1, h_2, \ldots . h_n .$$

The boundary conditions on this part of the sheet are applied at n points intermediate between the pivotal points, at polar angles

$$\tfrac{1}{2}h_1, \tfrac{1}{2}(h_2+h_1), \tfrac{1}{2}(h_3+h_2), \ldots . \tfrac{1}{2}(h_n+h_{n-1})$$

and at polar distances

$$d_1=\tfrac{1}{2}(d_0+d_2), d_3=\tfrac{1}{2}(d_2+d_4), \ldots . d_{2n-1}=\tfrac{1}{2}(d_{2n-2}+d_{2n}) ,$$

where $d_0=|\zeta_V|$ is the distance of the vortex from the origin.

The strength of the sheet is specified by the values of the derivative of the circulation with respect to the polar angle, $d\Delta\Phi/d\vartheta$, at the pivotal points:

$$g_j=-\frac{1}{KU}\frac{d\Delta\Phi}{d\vartheta}\bigg|_{\vartheta=h_j} \qquad j=1,2,\ldots n . \tag{11}$$

The strength of the starboard vortex is represented by

$$g=\frac{\Gamma}{KU} \tag{12}$$

and its position is at

$$\zeta_V=\bar{y}+i\bar{z}=d_0e^{ib} . \tag{13}$$

The coordinates $(\bar{y}_{2j}, \bar{z}_{2j})$ of the pivotal, and $(\bar{y}_{2j-1}, \bar{z}_{2j-1})$ of the intermediate, points now follow:

and

$$\left.\begin{aligned} \bar{y}_{2j}+i\bar{z}_{2j} &= \bar{y}+i\bar{z}-d_{2j}e^{i(b+h_j)} \\ \bar{y}_{2j-1}+i\bar{z}_{2j-1} &= \bar{y}+i\bar{z}-d_{2j-1}e^{i(b+\frac{1}{2}h_{j-1}+\frac{1}{2}h_j)} \end{aligned}\right\} \quad j=1,2,\ldots n. \tag{14}$$

This completes the specification of the configuration in the ζ-plane. Related quantities are now needed in the Z-plane.

The semi-span, s, is given by equation (8). If ε is small, the integrand has a weak zero at $t=0$, and if $\varepsilon=0{\cdot}5$ it has a square-root singularity at $t=1$. The transformation

$$t=1-5\xi^4+4\xi^5, \quad dt=-20\xi^3(1-\xi), \quad 0\leqslant\xi\leqslant 1$$

takes care of both difficulties. Equation (8) becomes

$$s=20\sin\varepsilon\pi\int_0^1\left(\frac{t^2}{1-t^2}\right)^{\varepsilon}(1-\xi)\xi^3 d\xi, \tag{15}$$

so that the integrand, as a function of ξ, has at least a linear zero at $t=0$, $\xi=1$ and at least a linear zero at $t=1$, $\xi=0$. Equation (15) was evaluated numerically by dividing the ξ-interval (0, 1) into tenths and using the Gaussian five-point formula in each.

The set of pivotal and intermediate points on the sheet is extended by adding the origin at one end and the position of the isolated vortex at the other, to give a sequence of points

$$\zeta_0=0\ ; \quad \zeta_j=\bar{y}_j+i\bar{z}_j, \quad j=1,2,\ldots 2n\ ; \quad \zeta_{2n+1}=\bar{y}+i\bar{z}.$$

Equation (7) defines a sequence of corresponding points Z_j in the Z-plane. It is convenient to refer these to the semi-span, s, so that we write

$$Z_0=s\ ; \quad Z_j=s(y_j+iz_j), \quad j=1,2,\ldots 2n\ ; \quad Z_{2n+1}=s(y+iz). \tag{16}$$

The points are then calculated in turn, writing (7) as

$$Z_{j+1}=Z_j+\int_{\zeta_j}^{\zeta_{j+1}}\left(\frac{t^2}{t^2+1}\right)^{\varepsilon}dt, \qquad j=0,1,\ldots 2n$$

$$=Z_j+(\zeta_{j+1}-\zeta_j)\int_0^1\left(\frac{t^2}{t^2+1}\right)^{\varepsilon}d\xi, \tag{17}$$

where $t=\zeta_j+\xi(\zeta_{j+1}-\zeta_j)$. The integration with respect to ξ was performed using the Gaussian five-point formula, on the basis that the points are closely spaced.

Since the boundary conditions (3) and (4) involve the quantities r and φ, we need the moduli and arguments of the points on the sheet in the Z-plane:

$$y_j+iz_j=b_je^{ic_j} \qquad j=1,2,\ldots 2n. \tag{18}$$

Derivatives along the sheet are approximated in the simplest way, giving, at the jth intermediate point:

$$\frac{1}{s}\frac{dr}{d\vartheta}\simeq\frac{b_{2j}-b_{2j-2}}{h_j-h_{j-1}}\qquad=f_{2j-1}\,, \tag{19}$$

$$\frac{d\theta}{d\vartheta}\simeq\frac{c_{2j}-c_{2j-2}}{h_j-h_{j-1}}\qquad=f_{2j}\,, \tag{20}$$

$$\frac{d\bar{r}}{d\vartheta}\simeq\frac{d_{2j}-d_{2j-2}}{h_j-h_{j-1}}\qquad=e_{2j-1} \tag{21}$$

and

$$\frac{d\bar{\sigma}}{d\vartheta}\simeq(d_{2j-1}^2+e_{2j-1}^2)^{\frac{1}{2}}=e_{2j} \tag{22}$$

for $j=1,2,\ldots n$, with $b_0=1$, $c_0=0$, and $h_0=0$. Here $\bar{\sigma}$ is the arc length along the sheet in the transformed plane.

We now need finite difference forms for the integrals in equation (10). Consider first the contribution of the source distribution on the transform of the wing. Setting $d=1$ and reducing the interval of integration by changing the sign of t in the negative half, we have

$$\int_{-id}^{id}\left|\left(\frac{t^2}{t^2+d^2}\right)^{\varepsilon}\right|\frac{dt}{\zeta-t}=2\zeta\int_0^{i\infty}\left|\left(\frac{t^2}{t^2+1}\right)^{\varepsilon}\right|\frac{dt}{\zeta^2-t^2}$$

$$=\pi i\zeta\int_0^1\frac{\left(\sin\frac{\pi\xi}{2}\right)^{2\varepsilon}\left(\cos\frac{\pi\xi}{2}\right)^{1-2\varepsilon}d\xi}{\zeta^2+\sin^2\frac{\pi\xi}{2}},$$

where $t=i\sin\frac{\pi\xi}{2}$. Since we do not need to evaluate this on the wing surface, the integrand is non-singular. It has weak zeros at the ends of the interval, but no special consideration was given to them. The interval (0, 1) in ξ was divided into tenths and the Gaussian five-point formula applied in each to evaluate the integral. If $\alpha_1,\ldots\alpha_5$ are the points and $\beta_1,\ldots\beta_5$ are the weights, such that

$$\int_0^1 F(t)dt\simeq\sum_1^5\beta_iF(\alpha_i)\,,$$

the values $\xi_k=(i+\alpha_j)/10$, $k=5i+j$, $i=0,1,\ldots 9$, $j=1,2,\ldots 5$ are chosen. Then, if

$$\gamma_k=\left(\sin\frac{\pi\xi_k}{2}\right)^{2\varepsilon}\left(\cos\frac{\pi\xi_k}{2}\right)^{1-2\varepsilon}\text{ and }\delta_k=\left(\sin\frac{\pi\xi_k}{2}\right)^2$$

we have

$$\int_{-id}^{id}\left|\left(\frac{t^2}{t^2+d^2}\right)^{\varepsilon}\right|\frac{dt}{\zeta-t}=\frac{\pi i\zeta}{10}\sum_{j=1}^{5}\beta_j\sum_{i=0}^{9}\frac{\gamma_{5i+j}}{\zeta^2+\delta_{5i+j}}. \tag{23}$$

Now consider the contribution from the vortex sheet and its image. At a general point ζ, we simply apply the trapezium rule, as in Ref. 1:

$$\int_0^{\vartheta_{\max}} \left(-\frac{d\Delta\Phi}{d\vartheta}\right)\left(\frac{1}{\zeta-\zeta(\vartheta)}-\frac{1}{\zeta+\bar{\zeta}(\vartheta)}\right)d\vartheta$$

$$=KU\sum_{j=1}^{n}\frac{g_j\bar{y}_{2j}(h_{j+1}-h_{j-1})}{(\zeta-\bar{y}_{2j}-i\bar{z}_{2j})(\zeta+\bar{y}_{2j}-i\bar{z}_{2j})} \tag{24}$$

where, conventionally, $h_0=0$ and $h_{n+1}=h_n$. This representation assumes that the integrand vanishes at $\vartheta=0$, which it does for $\zeta\neq 0$. In order to apply the Kutta-Joukowski condition at the leading edge, we also need a representation valid for $\zeta=0$.

The integrand on the left of (24) may well be infinite at $\vartheta=0$ if $\zeta=0$. Consider the first factor:

$$\frac{d\Delta\Phi}{d\vartheta}\sim\frac{d\Delta\Phi}{d\bar{\sigma}}=\frac{d\Delta\Phi}{d\sigma}\frac{d\sigma}{d\bar{\sigma}}=\frac{d\Delta\Phi}{d\sigma}\left|\frac{dZ}{d\zeta}\right| \sim\frac{d\Delta\Phi}{d\sigma}|\zeta|^{2\varepsilon}\sim\frac{d\Delta\Phi}{d\sigma}\vartheta^{2\varepsilon}.$$

Now, if the Kutta-Joukowski condition is satisfied, $d\Delta\Phi/d\sigma$ must be finite at the leading edge, since it represents the difference in tangential velocity across the sheet. Further, if the condition of continuity of pressure, equation (4), is satisfied at the leading edge, $d\Delta\Phi/d\sigma$ is non-zero there. Hence

$$\frac{d\Delta\Phi}{d\vartheta}\sim\vartheta^{2\varepsilon}.$$

The second factor is straightforward:

$$\frac{1}{\zeta(\vartheta)}+\frac{1}{\bar{\zeta}(\vartheta)}=\frac{2\mathscr{R}(\zeta)}{|\zeta|^2}\sim\frac{1}{\vartheta}.$$

Hence the integrand tends to infinity like $\vartheta^{2\varepsilon-1}$. If the integrand is written in the form

$$f=k_1\vartheta^{2\varepsilon-1}+k_2$$

we find

$$\int_0^{h_1} f(\vartheta)d\vartheta=\frac{k_1h_1^{2\varepsilon}}{2\varepsilon}+k_2h_1$$

$$=h_1f_1+\left(\frac{1}{2\varepsilon}-1\right)\frac{h_1^{2\varepsilon}(f_2-f_1)}{h_2^{2\varepsilon-1}-h_1^{2\varepsilon-1}}$$

where $f_1=f(h_1)$ and $f_2=f(h_2)$. We now apply this rule over the first interval and the trapezium rule over the remainder to obtain:

$$\frac{1}{KU}\int_0^{\vartheta_{\max}}\left(-\frac{d\Delta\Phi}{d\vartheta}\right)\left(\frac{1}{\zeta(\vartheta)}+\frac{1}{\bar{\zeta}(\vartheta)}\right)d\vartheta=\frac{(h_1+h_2)g_1\bar{y}_2}{\bar{y}_2^2+\bar{z}_2^2}+$$

$$+\left(\frac{1}{2\varepsilon}-1\right)\frac{2h_1^{2\varepsilon}}{h_2^{2\varepsilon-1}-h_1^{2\varepsilon-1}}\left(\frac{g_2\bar{y}_4}{\bar{y}_4^2+\bar{z}_4^2}-\frac{g_1\bar{y}_2}{\bar{y}_2^2+\bar{z}_2^2}\right)+\sum_{j=2}^{n}\frac{g_j\bar{y}_{2j}(h_{j+1}-h_{j-1})}{\bar{y}_{2j}^2+\bar{z}_{2j}^2}, \tag{25}$$

with $h_{n+1}=h_n$.

3.2. *Expression of the Boundary Conditions.*

Since the flow separates at the leading edge, the Kutta-Joukowski condition must be applied there. This implies a finite velocity in the cross-flow plane and therefore a stagnation point at the origin of the transformed plane. Putting $dW/d\zeta=0$ for $\zeta=0$ in (10), and using (23) and (25), we find

$$2\pi a=\frac{2g\bar{y}}{\bar{y}^2+\bar{z}^2}+\sum_{j=1}^{n}\frac{g_j\bar{y}_{2j}A_j}{\bar{y}_{2j}^2+\bar{z}_{2j}^2}, \tag{26}$$

where we have divided through by $KUi/2\pi$, set $\alpha/K=a$, used (12) and (13) for Γ and ζ_V, and introduced

$$A_1=h_1+h_2-\frac{(1-2\varepsilon)h_1^{2\varepsilon}}{\varepsilon(h_2^{2\varepsilon-1}-h_1^{2\varepsilon-1})},\quad A_2=h_3-h_1+\frac{(1-2\varepsilon)h_1^{2\varepsilon}}{\varepsilon(h_2^{2\varepsilon-1}-h_1^{2\varepsilon-1})},$$

$$A_j=h_{j+1}-h_{j-1}\text{ for }3\leqslant j\leqslant n.$$

The condition of zero total force on the vortex and cut is given by equation (6). We multiply through by $dZ/d\zeta$ at V and obtain:

$$\lim_{\zeta\to\zeta_V}\left(\frac{dW}{d\zeta}-\frac{\Gamma}{2\pi i}\frac{dZ}{d\zeta}\frac{1}{Z-Z_V}\right)=KU\frac{2\bar{Z}_V-\bar{Z}_E}{s}\frac{dZ}{d\zeta}\bigg|_V. \tag{27}$$

Now the only term in (10) which is singular as $\zeta\to\zeta_V$ is $\Gamma/2\pi i(\zeta-\zeta_V)$, so we need to consider

$$\frac{1}{\zeta-\zeta_V}-\frac{dZ}{d\zeta}\frac{1}{Z-Z_V} \tag{28}$$

for ζ near ζ_V. The Taylor series gives

$$Z-Z_V=(\zeta-\zeta_V)\frac{dZ}{d\zeta}\bigg|_V+\tfrac{1}{2}(\zeta-\zeta_V)^2\frac{d^2Z}{d\zeta^2}\bigg|_V+\ldots$$

$$\frac{dZ}{d\zeta}=\frac{dZ}{d\zeta}\bigg|_V+(\zeta-\zeta_V)\frac{d^2Z}{d\zeta^2}\bigg|_V+\ldots$$

therefore

$$\frac{\zeta-\zeta_V}{Z-Z_V}\frac{dZ}{d\zeta}=1+\tfrac{1}{2}(\zeta-\zeta_V)\frac{d^2Z/d\zeta^2}{dZ/d\zeta}\bigg|_V+\ldots.$$

Hence the limit of (28) as $\zeta\to\zeta_V$ is

$$-\frac{1}{2}\frac{d^2Z/d\zeta^2}{dZ/d\zeta}\bigg|_V=-\frac{\varepsilon}{\zeta_V(1+\zeta_V^2)},\text{ by (7)}.$$

Introducing FKU for the difference between the right and left-hand sides of (27), we can use this limit with equations (10), (23) and (24) to write

$$F=\frac{2(y-iz)-(y_{2n}-iz_{2n})}{s}\left(\frac{(\bar{y}+i\bar{z})^2}{1+(\bar{y}+i\bar{z})^2}\right)^{\varepsilon}+ia-$$

$$-\frac{ig}{4\pi}\left(\frac{1}{\bar{y}}+\frac{2\varepsilon}{(\bar{y}+i\bar{z})\,(1+(\bar{y}+i\bar{z})^2)}\right)-\frac{(\bar{y}+i\bar{z})\cos\varepsilon\pi}{10}\sum_{j=1}^{5}\beta_j\sum_{k=0}^{9}\frac{\gamma_{5k+j}}{(\bar{y}+i\bar{z})^2+\delta_{5k+j}}+$$

$$+\frac{i}{2\pi}\sum_{j=1}^{n}\frac{g_j\bar{y}_{2j}(h_{j+1}-h_{j-1})}{(\bar{y}+i\bar{z}-\bar{y}_{2j}-i\bar{z}_{2j})\,(\bar{y}+i\bar{z}+\bar{y}_{2j}-i\bar{z}_{2j})}. \tag{29}$$

Then the required condition is that the real and imaginary parts of F should be zero.

To express the conditions that the sheet is a stream surface (3), with no jump in pressure across it (4), we need expressions for the components of the cross-flow velocity normal and tangential to the sheet at the intermediate points. It is the mean velocity across the sheet which is required and this is what is given by the formulation (10) applied at a point of the sheet. Although it is velocities in the Z-plane which appear in equations (3) and (4), it is more convenient to work in the ζ-plane. Let v_{t_m} and v_n be the mean tangential and normal components of velocity, so that

$$v_{t_m}-iv_n=\frac{dW}{d\bar{\sigma}}=\frac{dW}{d\zeta}\frac{d\zeta}{d\bar{\sigma}}. \tag{30}$$

The first factor on the right is given by (10), in conjunction with (23) and (24). On the sheet

$$\zeta=\zeta_V-\bar{r}e^{i(b+\vartheta)}$$

and so

$$\frac{d\zeta}{d\vartheta}=\frac{\zeta-\zeta_V}{\bar{r}}\left(\frac{d\bar{r}}{d\vartheta}+i\bar{r}\right).$$

$d\bar{r}/d\vartheta$ and $d\bar{\sigma}/d\vartheta$ at the intermediate points are given by (21) and (22), so that, at the jth intermediate point:

$$\frac{d\zeta}{d\bar{\sigma}}=\frac{d\zeta}{d\vartheta}\Big/\frac{d\bar{\sigma}}{d\vartheta}=\frac{(\bar{y}_{2j-1}+i\bar{z}_{2j-1}-\bar{y}-i\bar{z})\,(e_{2j-1}+id_{2j-1})}{d_{2j-1}e_{2j}} \tag{31}$$

From (10), (23) and (24), at the jth intermediate point:

$$\frac{1}{KU}\frac{dW}{d\zeta}=-ia+(\bar{y}_{2j-1}+i\bar{z}_{2j-1})\frac{\cos\varepsilon\pi}{10}\sum_{l=1}^{5}\beta_l\sum_{k=0}^{9}\frac{\gamma_{5k+l}}{(\bar{y}_{2j-1}+i\bar{z}_{2j-1})^2+\delta_{5k+l}}-$$

$$-\frac{ig\bar{y}}{\pi(\bar{y}_{2j-1}+i\bar{z}_{2j-1}-\bar{y}-i\bar{z})\,(\bar{y}_{2j-1}+i\bar{z}_{2j-1}+\bar{y}-i\bar{z})}-$$

$$-\frac{i}{2\pi}\sum_{k=1}^{n}\frac{g_k\bar{y}_{2k}(h_{k+1}-h_{k-1})}{(\bar{y}_{2j-1}+i\bar{z}_{2j-1}-\bar{y}_{2k}-i\bar{z}_{2k})(\bar{y}_{2j-1}+i\bar{z}_{2j-1}+\bar{y}_{2k}-i\bar{z}_{2k})}. \tag{32}$$

Equations (30), (31) and (32) express the required velocity components.

The condition of zero pressure jump (4) can be written, at the jth intermediate point, as

$$\left.\frac{\Delta\Phi}{KU}\right|_{P_j}=\left(-\frac{1}{KU}\frac{d\Delta\Phi}{d\vartheta}\right)_{P_j}\varepsilon_j, \tag{33}$$

where

$$\begin{aligned}\varepsilon_j&=\frac{d\vartheta}{d\sigma}\left(s\frac{v_{t_m}}{KU}\frac{d\bar{\sigma}}{d\sigma}-r\frac{dr}{d\sigma}\right)\text{at } P_j\\&=\left.\frac{d\zeta}{dZ}\right|^2 s\left(\frac{v_{t_m}}{KU}-\frac{r}{s}\frac{dr}{d\vartheta}\middle/\frac{d\bar{\sigma}}{d\vartheta}\right)\middle/\frac{d\bar{\sigma}}{d\vartheta}\text{ at } P_j\\&=\frac{s}{e_{2j}}\left|\frac{1+(\bar{y}_{2j-1}+i\bar{z}_{2j-1})^2}{(\bar{y}_{2j-1}+i\bar{z}_{2j-1})^2}\right|^{2\varepsilon}\left(\left.\frac{v_{t_m}}{KU}\right|_{P_j}-\frac{b_{2j-1}sf_{2j-1}}{e_{2j}}\right),\end{aligned} \tag{34}$$

where v_{t_m}/KU at P_j follows from (30)–(32). The n equations of the form of (33), together with the Kutta-Joukowski condition (26), are used to determine the $n+1$ quantities g and g_j, $j=1,2,\ldots n$, for fixed geometrical quantities. The procedure used is an iterative one in which values of g and g_j derived at the previous step are used to find v_{t_m}/KU at the intermediate points, and hence the values of ε_j in (33). The set of equations (33) are written as linear equations in the values of $d\Delta\Phi/d\vartheta$ at the intermediate points and solved explicitly as follows. Let

$$\lambda_j=-\left.\frac{1}{KU}\frac{d\Delta\Phi}{d\vartheta}\right|_{P_j}. \tag{35}$$

Now

$$\left.\frac{\Delta\Phi}{KU}\right|_{P_j}=g+\int_{\frac{1}{2}(h_{j-1}+h_j)}^{h_n}\left(-\frac{1}{KU}\frac{d\Delta\Phi}{d\vartheta}\right)d\vartheta. \tag{36}$$

This integral is then approximated by the trapezium rule over the intervals between the intermediate points and by assuming the integrand is constant over the interval between the nth intermediate point and the end of the sheet. Hence (35) and (36) enable us to write $\Delta\Phi$ at P_j as a linear combination of g and λ_i, and the set of equations (33) can be written as

$$4g+(h_{j+1}-h_{j-1})\lambda_j+\sum_{i=j+1}^{n}(h_{i+1}+h_i-h_{i-1}-h_{i-2})\lambda_i=4\lambda_j\varepsilon_j, \tag{37}$$

for $j=1,2,\ldots n$, where $h_0=0$ as before, but now $h_{n+1}=2h_n-h_{n-1}$.

The set of n equations (37) can be solved for λ_j in terms of g. Starting with the last, the solution is

$$\left.\begin{aligned} &\lambda_n = 4g/\mu_n\,, \\ &\lambda_j = (\mu_{j+1}+\nu_{j+1})\lambda_{j+1}/\mu_j \qquad j=n-1, n-2, \ldots 1 \\ &\mu_j = 4\varepsilon_j - h_{j+1} + h_{j-1} \qquad j=1,2,\ldots n \\ &\nu_j = h_{j+1}+h_j-h_{j-1}-h_{j-2} \qquad j=2,3,\ldots n\,. \end{aligned}\right\} \tag{38}$$

where

and

Linear interpolation and extrapolation now give the g_j in terms of the λ_j thus:

$$\left.\begin{aligned} &g_j = [(h_j-h_{j-1})\lambda_{j+1}+(h_{j+1}-h_j)\lambda_j]/(h_{j+1}-h_{j-1}) \qquad j=1,2,\ldots n-1 \\ &g_n = [(h_{n+1}-h_{n-2})\lambda_n-(h_n-h_{n-1})\lambda_{n-1}]/(h_n-h_{n-2}) \end{aligned}\right\} \tag{39}$$

and

where $h_{n+1}=2h_n-h_{n-1}$. Equations (38) and (39) together express the quantities g_i in the form

$$g_j = B_j g\,, \tag{40}$$

where the B_j can readily be written down (*see* equation (A.7)). Introducing these into (26) we obtain an equation for g:

$$g\left(\frac{2\bar{y}}{\bar{y}^2+\bar{z}^2}+\sum_{j=1}^{n}\frac{A_jB_j\bar{y}_{2j}}{\bar{y}_{2j}^2+\bar{z}_{2j}^2}\right)=2\pi a\,, \tag{41}$$

where the A_j are defined after equation (26). Equation (41) yields a value of g and then (40) gives values for g_j. These values are then used to recalculate the ε_j and the iteration is repeated. When the values of g and g_j found are little altered from the previous cycle, the Kutta-Joukowski condition and the condition of continuity of pressure are regarded as being satisfied.

The final condition to be expressed in a form suitable for computation is the condition (3) that the vortex sheet is a stream surface. We first replace (3) by the equivalent condition in the transformed (ζ) plane:

$$\frac{v_n}{KU}=-\left|\frac{dZ}{d\zeta}\right|\frac{r}{s}\sin\varphi=-s\left(\frac{r}{s}\right)^2\frac{d\theta}{d\vartheta}\Big/\frac{d\bar{\sigma}}{d\vartheta}\,, \tag{42}$$

using the standard expression $\sin\varphi = rd\theta/d\sigma$. Equations (30)–(32) provide the values of v_n/KU at the intermediate points and the values of the right-hand side at the same points follow from (15), (18), (20) and (22). What is needed is a method for using the discrepancy that will exist between the two sides of (42) at any stage of the calculation to modify the shape of the sheet. If the tangent to the sheet at the jth intermediate point were rotated anti-clockwise through an angle χ_j, the mean velocity along the new normal would be

$$v_n\cos\chi_j - v_{t_m}\sin\chi_j\,.$$

If this new direction is such that (42) is satisfied,

$$\frac{v_n}{KU}\Big|_{P_j}\cos\chi_j-\frac{v_{t_m}}{KU}\Big|_{P_j}\sin\chi_j=-sb_{2j-1}^2f_{2j}/e_{2j}\,.$$

Since we can only think in terms of small changes to the shape of the sheet, we can regard χ_j as small and solve this equation for it, giving

$$\chi_j = \left(\frac{v_n}{KU} \bigg|_{P_j} + \frac{sb_{2j-1}^2 f_{2j}}{e_{2j}} \right) \Big/ \frac{v_{tm}}{KU} \bigg|_{P_j} . \tag{43}$$

The final step is to convert this rotation of the tangent at the intermediate points to changes in the polar distances from the vortex to the pivotal points. Suppose each distance, d_{2j}, is increased by an amount δ_j, as in Fig. 4, with the pivotal points Q_j moving to Q'_j. The tangent at the jth intermediate point is taken to be parallel to $Q_{j-1}Q_j$, so that the angle between $Q_{j-1}Q_j$ and $Q'_{j-1}Q'_j$ is the χ_j of equation (43), as shown in Fig. 4. The elementary geometry needed is most conveniently expressed in vector notation. Denote $\mathbf{VQ}_{j-1}$ by $\mathbf{a}$, $\mathbf{Q}_{j-1}\mathbf{Q}'_{j-1}$ by $\lambda\mathbf{a}$, $\mathbf{VQ}_j$ by $\mathbf{b}$ and $\mathbf{Q}_j\mathbf{Q}'_j$ by $\mu\mathbf{b}$. Then $\mathbf{Q}_{j-1}\mathbf{Q}_j$ is $\mathbf{b}-\mathbf{a}$ and $\mathbf{Q}'_{j-1}\mathbf{Q}'_j$ is $(1+\mu)\mathbf{b}-(1+\lambda)\mathbf{a}$. If $\mathbf{k}$ is a unit vector out of the plane of the figure:

$$(\mathbf{b}-\mathbf{a}) \wedge ((1+\mu)\mathbf{b}-(1+\lambda)\mathbf{a}) = |\mathbf{b}-\mathbf{a}||(1+\mu)\mathbf{b}-(1+\lambda)\mathbf{a}|\mathbf{k} \sin \chi_j , \tag{44}$$

$$\mathbf{a} \wedge \mathbf{b} = |\mathbf{a}||\mathbf{b}|\mathbf{k} \sin (h_j - h_{j-1}) , \tag{45}$$

$$|\mathbf{b}-\mathbf{a}|^2 = (\mathbf{b}-\mathbf{a})(\mathbf{b}-\mathbf{a}) = \mathbf{bb}+\mathbf{aa}-2\mathbf{ab} \tag{46}$$

and

$$\mathbf{ab} = |\mathbf{a}||\mathbf{b}| \cos (h_j - h_{j-1}) . \tag{47}$$

The right-hand side of (44) is already a small quantity of order χ_j, so the difference between the first two factors, which is also of order χ_j, can be ignored. Equations (46) and (47) then allow us to reduce the right-hand side of (44) to

$$(|\mathbf{b}|^2+|\mathbf{a}|^2-2|\mathbf{a}||\mathbf{b}| \cos (h_j - h_{j-1}))\mathbf{k}\chi_j + 0(\chi_j^2) .$$

Expanding the vector product on the left-hand side of (44) and using (45), we reduce it to

$$(\lambda-\mu)|\mathbf{a}||\mathbf{b}| \quad \sin (h_j - h_{j-1}) .$$

Equating these two expressions and reverting to the scalar notation we find

$$\mu = \frac{\delta_j}{d_{2j}} = \frac{\delta_{j-1}}{d_{2j-2}} - \frac{d_{2j}^2 + d_{2j-2}^2 - 2d_{2j}d_{2j-2} \cos (h_j - h_{j-1})}{d_{2j}d_{2j-2} \sin (h_j - h_{j-1})} \chi_j . \tag{48}$$

Since the beginning of the sheet is fixed at the origin of the ζ-plane, $\delta_0 = 0$. Equation (48), with χ_j given by (43), enables us to calculate $\delta_1, \delta_2, \ldots \delta_n$ in turn. The way in which this and the other relations obtained in this sub-section are used is explained in the following sub-section.

3.3. *Iteration Scheme.*

The problem is to determine the flow field of a given wing at given incidence. The wing and incidence are specified by values of ε and a. The flow field is determined by the position and strength of the vortex, i.e. $\bar{y}$, $\bar{z}$ and g, and by the shape and strength of the sheet, i.e. sets of d_{2j} and g_j appropriate to a set of angles h_j $(j = 1,2, \ldots n)$. The method consists of three nested iteration procedures.

The innermost iteration leaves the position of the vortex and the shape of the sheet unchanged and determines values of g and g_j which satisfy the Kutta-Joukowski condition at the leading edge exactly and satisfy the condition of continuity of pressure along the sheet to within a prescribed tolerance. The second iteration leaves the shape of the vortex sheet unchanged and adjusts the position of the isolated vortex until the condition of zero overall force on the vortex and cut is satisfied, again within a

certain tolerance. Throughout this process the innermost iteration is used to change g and g_j in step with the changes in $\bar{y}$ and $\bar{z}$. The outermost iteration modifies the shape of the sheet to make it conform more closely to a stream surface of the threedimensional flow. These three iterative procedures will now be described in more detail.

An initial approximate solution can be taken either from Ref. 1 if the wing is very thin or from a solution already obtained for some slightly different value of a or ε. If solutions are being generated from a sequence of values a or ε, a good initial approximation is obtained by extrapolating linearly from the two previous solutions in the sequence. Most of the results described in this Report were obtained sequentially in this way.

All the geometrical quantities needed are derived from the equations of Sub-Section 3.1. The innermost iteration then starts. In principle, the mean tangential velocity at the intermediate points is calculated (equations (30), (31) and (32)) and used to form $\{\varepsilon_j\}$ (34). These values are used to give $\{\mu_j\}$ and $\{\nu_j\}$ and hence $\{B_j\}$ (38)–(40). Equation (41) determines g and (40) determines $\{g_j\}$. The value of g is compared with the initial approximation and, unless the change is less than a tolerance e', the cycle of operations is repeated. In practice, the method uses a number of other intermediate quantities to speed up the procedure as explained in Appendix I.

The next step is to adjust the position of the vortex $(\bar{y}, \bar{z})$ until the modulus of the complex function $F(\bar{y}, \bar{z})$, proportional to the force on the vortex and the cut, is less than a prescribed tolerance, or until the vortex is sufficiently close to a minimum of $|F|$. F is given by equation (29) in which the quantities g and $\{g_j\}$ depend on $(\bar{y}, \bar{z})$ through the iteration process just described. The method chosen exploits the fact that, near the vortex location sought, the surface $|F(\bar{y}, \bar{z})|$ resembles a closed valley with its long axis roughly in the direction of the axis of $\bar{z}$. This emerged from the calculations of Ref. 1. We seek the bottom of the valley, assuming that F will be zero there. Fig. 5 illustrates the procedure. First, we march across the valley, i.e. parallel to the axis of $\bar{y}$, calculating F at each step and stopping when $|F|$, after initially decreasing, begins to increase. The conditional minimum along this line $\bar{z} = \text{constant}$ is located by interpolation and stored. We then march across the valley along another line of constant $\bar{z}$, and again store the conditional minimum. We then march along the line joining the two conditional minima until a third (conditional) minimum is reached. We assume that this point is within a few steps of the actual minimum sought. If the initial steps have to be rather large, because the location of the valley floor is uncertain, the set of three marches can be repeated, starting from the approximate minimum found, with a reduced length of step. In this way we can expect to get as near to the minimum of $|F(\bar{y}, \bar{z})|$ as we please. If at any point the modulus of F falls below a tolerance f', we seek no further. A minor complication arises in that, when the vortex is moved, the part of the sheet closest to it has to be moved with it, whereas the further end of the sheet must remain attached to the leading edge. The first k of the distances $\{d_{2j}\}$ are adjusted each time the vortex is moved, as described in Ref. 1.

The scheme requires something akin to the continuity of $F(\bar{y}, \bar{z})$. Since F depends on the iteration which determines g and $\{g_j\}$, it is certainly not continuous in the classical sense. Nonetheless, provided the tolerance e' is small enough in relation to the step size, F behaves sufficiently like a continuous function for the scheme to work successfully. A feature of its occasional failure to work is the occurrence of three consecutive values of $|F|$ with the middle one higher than the other two. If this happens a diagnostic message 'local maximum' is printed and the computer program jumps to the next part of the calculation.

Apart from such hazards, the calculation has now positioned the isolated vortex close to the point at which the condition of zero total force is satisfied, with a circulation distribution satisfying the Kutta condition and the condition of continuity of pressure across the sheet. The next step is to change the form of the sheet so that the condition on the normal velocity is more closely satisfied. Equation (48) in the previous section gives the changes $\{\delta_j\}$ that would be needed in the $\{d_{2j}\}$ to satisfy the condition, if these really were small. There are three possibilities:

(a) the largest of the proportionate changes called for in the polar distances may be so small (less than a parameter g') that we can regard the solution as having been obtained,

(b) it may be larger than this but still small enough (less than a parameter h') for the whole of the change to be applied without seriously violating the assumption on which it was calculated, or

(c) it may be larger still.

In case (a) the calculation for the current values of a and ε is complete. In case (b) the changes called for are applied to the polar distances and the entire calculation is repeated. In case (c) the changes called for are scaled down so that the largest of them is equal to h' and these scaled changes are applied before returning to the beginning of the calculation. The size of h' is regulated by the need to suppress a tendency for the sheet to oscillate in and out. If the change called for in the last polar distance, d_{2n}, is in the opposite sense to that called for on the last passage through this iteration, the maximum permitted proportional change, h', is halved before proceeding.

A somewhat simplified flow diagram of the computer program which performs this calculation is given in Fig. 6, with the intention of making clearer the description of the course of the calculation. The subroutine R referred to in Fig. 6 is laid out in Fig. 7. Note that R has a normal exit and an exit to the fixed point A at the top right of Fig. 6. The conventions of Ref. 26 have been followed in that the flow is from top to bottom and from left to right unless arrows indicate the contrary, and that flows merge at T-junctions but do not interact at intersections.

3.4. *Choice of Parameters.*

It is clear from the description of the numerical treatment given above that the solutions obtained from the iteration scheme will depend, not only on the real parameters ε and a (representing the thickness and incidence of the wing), but also on the tolerances used in the iterations, on the extent of the finite part of the vortex sheet and on the number of points used to define this part of the vortex sheet. The choice of these incidental parameters will be described here.

In the earlier work on the flat plate it was concluded that an angular extent of the finite part of the vortex sheet of 157 degrees was adequate, where this was measured about the isolated vortex in the transformed plane. This conclusion was based on the very small changes in vortex position, in lift and in overall circulation, and the very local changes in pressure on the wing, that were produced when one or two further complete turns of the sheet were added. It was also found that doubling the number of points used to define the sheet produced small changes in its shape, when the sheet extended for one and a half turns about the vortex and the number of pivotal points rose from 21 to 42. Consequently a similar distribution of pivotal points was used, requiring 11 to define the present sheet extending for 157 degrees instead of 21 to define the sheet of extent 517 degrees in Ref. 1. The values of the angular coordinates h_j are given in Table 1. The parameter k was taken equal to $n=11$.

TABLE 1

Values of angular coordinates of pivotal points.

j	1	2	3	4	5	6	7	8	9	10	11
h_j	0·12	0·25	0·39	0·54	0·70	0·87	1·05	1·27	1·57	2·04	2·75

The tolerances that must be considered are:

e', the tolerance on the change in the strength g of the isolated vortex;

f', the tolerance on the quantity $|F|$ proportional to the force on the isolated vortex and the cut;

g', the tolerance on the largest proportional change called for in the $\{d_{2j}\}$; and

a', the size of the step by which the isolated vortex is moved in the search for a minimum of $|F|$.

Unless the first of these, e', is small enough, the search procedure for the minimum of $|F|$ will fail, as discussed in Sub-Section 3.3. Hence, so long as the search proceeds satisfactorily we can assume e' is small enough. A value of 10^{-3} was used for the bulk of the cases computed and found satisfactory. In Ref. 1, it was the largest of the changes in the $\{g_j\}$ that was inspected, with a tolerance of 1 or 2×10^{-4}.

Since the largest of the $\{g_j\}$ is between 5 and 10 times smaller than g, the levels of accuracy are comparable.

The second tolerance, f', can be set to zero, and in some cases it was. The search for the minimum of $|F|$ then proceeds through all the stages set out in Sub-Section 3.3. However, this is wasteful if all the values of $|F|$ being found are small, so it is more economical to use a non-zero value of f'. In the bulk of the cases calculated f' was taken as 10^{-3}. In Ref. 1, the corresponding tolerance was 10^{-5} on a quantity equivalent to $|F|^2$, so the present calculations are at least as accurate as the earlier ones in this respect.

With $f'=10^{-3}$ the search procedure usually terminated when $|F|$ fell below f'. However, in some cases the approximate minimum of $|F|$ was located and found to be larger than f'. In such cases it is the length of the step, a', that governs the accuracy. For the present calculations a' was chosen to be 10^{-3}, and we should expect that errors in vortex position arising from failure to satisfy exactly the condition of zero overall force would be of the same order.

The remaining tolerance, g', was taken to be 2×10^{-3}. This is the lower of the two values used in Ref. 1 for the same quantity. As a check on the adequacy of this level, the value of

$$c=\sum_{j=1}^{n}\chi_j^2, \tag{49}$$

where χ_j is defined in equation (43), is printed. This gives a direct measure of the error made in satisfying the normal velocity condition approximately. In the solutions calculated c did not exceed 6×10^{-5}, which, with $n=11$, corresponds to a mean error $|\chi_j|$ in the direction of the tangent to the sheet of $2{\cdot}3\times10^{-3}$ or 0·13 degrees.

4. *Results.*

Eight sequences of solutions were obtained, in each of which either the thickness, ε, or the incidence, a, was held constant while the other was changed in steps of uniform size. The first sequence was for $\varepsilon=0{\cdot}5$, corresponding to $\delta=0$, and served to check that the present calculation was consistent with that of Ref. 1 for flat plates.

The next three sequences were for fixed values of $a=0{\cdot}5$, 1·0 and 1·5, with ε decreasing from 0·5 in steps of 0·01. At each value of a it became difficult to obtain solutions at the smaller values of ε and each sequence terminates with ε just above 0·1, i.e. δ just less than 144 degrees.

The final four sequences were for fixed values of $\varepsilon=0{\cdot}41\dot{6}$, $0{\cdot}\dot{3}$, 0·25 and $0{\cdot}1\dot{6}$, corresponding to $\delta=30$, 60, 90 and 120 degrees. For each value of ε a starting solution was obtained by interpolating in the sequence mentioned above with $a=1$ and ε varying. Then a was varied upwards and downwards from 1 in steps of 0·02. No difficulty was found in proceeding to larger incidences, the sequences usually terminating at a stage when the computer time requested was exhausted. Convergence difficulties were found at small values of a, as in Ref. 1. In fact, for $\varepsilon=0{\cdot}5$ the sequence terminated at almost the same value of a as in Ref. 1. The lowest value of a that could be reached is different for different values of ε, but too much emphasis should not be placed on the apparently irregular variation with ε, as no very strenuous efforts were made to obtain convergence at lower values of a.

The principal parameters of the solution in the eight sequences of results are listed in Tables 2–9. In each table the first two parameters shown against the current value of a (or ε) are the coordinates (y, z) of the isolated vortex in the physical, cross-flow, plane, referred to the semi-span, s, as unit of length. The second two parameters are the circulation of the isolated vortex, Γ, and of the finite part of the sheet, Γ_s; in each case referred to KUs, where K is the tangent of half the apex angle of the wing. The final parameter is the coefficient of normal force, C_N, divided by K^2. The factors K are those needed to produce quantities which depend on $a\,(=\alpha/K)$ and ε only. By equation (12) with an appropriate factor d introduced, we have

$$\frac{\Gamma}{KUs}=\frac{gd}{s}, \tag{50}$$

where s (or s/d) is given by (15). Using equation (11) and integrating by the trapezium rule we have

$$\frac{\Gamma_s}{KUs} = -\frac{d}{s}\frac{1}{KUd}\int_0^{\vartheta_{max}} \frac{d\Delta\Phi}{d\vartheta}\,d\vartheta$$

$$= \frac{d}{2s}\sum_{j=1}^{n}(h_{j+1}-h_{j-1})g_j, \text{ with } h_0=0 \text{ and } h_{n+1}=h_n\,. \tag{51}$$

The normal force is given by (B.7).

The procedure described above for obtaining the solutions sequentially suggests that the solutions for $\varepsilon = 0{\cdot}41\dot{6}$, $0{\cdot}\dot{3}$, $0{\cdot}25$ and $0{\cdot}1\dot{6}$ for $a = 0{\cdot}5$ and $1{\cdot}5$ were each obtained along two independent paths in the (ε, a) plane. In fact only for $\varepsilon = 0{\cdot}25$ was the value of ε exactly the same, so there are just two comparisons that can be made without interpolation. They are given in Table 10.

TABLE 10

Comparison of Solutions Reached along Independent Paths.

Proceeding along	At the point	y	z	g	C_N/K^2
$a = 1{\cdot}5$	$\varepsilon = 0{\cdot}25$	0·9117	0·3443	2·5343	12·776
$\varepsilon = 0{\cdot}25$	$a = 1{\cdot}5$	0·9118	0·3443	2·5343	12·776
$a = 0{\cdot}5$	$\varepsilon = 0{\cdot}25$	0·9707	0·1137	0·4956	2·8796
$\varepsilon = 0{\cdot}25$	$a = 0{\cdot}5$	0·9717	0·1116	0·4926	2·8723

In view of the differences between the entries for $a = 0{\cdot}5$, those for $a = 1{\cdot}5$ must be regarded as coincidentally close. The difference in vortex position for $a = 0{\cdot}5$ is consistent with that expected in Sub-Section 3.4. The values of g and C_N/K^2 are fairly closely linked to those of y and z, so their agreement for $a = 1{\cdot}5$ is not surprising. The values for $a = 0{\cdot}5$ indicate how errors in y and z affect the remaining quantities.

4.1. *Sheet Shape and Vortex Position.*

The effect of the thickness of the wing on the shape of the vortex sheet and the position of the isolated vortex is illustrated in Fig. 8. The three parts of the figure are for different fixed values of the incidence parameter, a, and each part of the figure shows the effect of varying the edge angle, δ, of the wing from zero to 120 degrees.

As the thickness increases, the size of the leading-edge vortex is reduced. This is associated with a reduction in the circulation about the vortex (Tables 7–9 or Fig. 13); and corresponds to a reduction in the strength of the singularity found at the leading edge in the attached flow (v. Appendix III). The shrinking of the sheet towards the leading edge implies a marked outboard movement of the isolated vortex as the thickness increases. Associated with the outboard movement of the isolated vortex is a vertical movement which is upward for the thinner wings and downward for the thicker wings. This can be regarded as the resultant of an upward trend from the displacement effect of the thickness and a downward trend from the shrinkage of the sheet towards the leading edge. It is only at the largest of the

three incidences shown that increasing thickness appears to increase the vertical extent of the sheet. The outward movement of the isolated vortex as the thickness increases is associated with an increased lateral projection of the vortex sheet beyond the leading edge, in spite of the general shrinkage.

This goes with a marked change in the shape of the sheet near the leading edge, seen most clearly in Fig. 8c, for the largest incidence. As the thickness increases, the curvature of the sheet near the leading edge falls, changing sign for the thickest wing, as seen more clearly in Fig. 9b. This appears to arise because the vortex sheet must leave the leading edge in a direction tangential to the lower surface. The necessity for this initial direction follows from an argument like that of Ref. 27. In the present calculations no restriction was placed on the initial direction of the vortex sheet and there is no feature of the transformed plane which could attract the sheet to this direction (Fig. 2a). The calculated shapes arose unambiguously from the calculation procedure described. For a smooth sheet to leave the lower surface of a thick wing tangentially and subsequently project well beyond the leading edge, its curvature near the edge must be small, or negative. The present calculations do not tell us whether the curvature at the leading edge itself is finite or, as appears likely for the flat plate, infinite.

In Fig. 9, the effect of varying incidence on the vortex formed on two thick wings is shown. For zero thickness the development is familiar[1]. The scale of Fig. 9 is large enough for the actual pivotal points to be indicated on the sheet and these are shown for two values of a in Fig. 9a and three in Fig. 9b. They demonstrate how close to the leading edge the calculations extend and how closely the calculation reproduces the tangency to the lower surface of the wing. It is curious that the vortex positions for $\delta = 90$ degrees (Fig. 9a) lie very close to a straight line through the leading edge, for all but the smallest of the values of a for which solutions were found. This contrasts with the apparently tangential approach of the isolated vortex to the leading edge for zero thickness, shown in Ref. 1 and Fig. 10a. The departure from the straight line for small a might have been attributed to a numerical error, were it not reproduced for rather larger values of a for $\delta = 120$ degrees in Fig. 9b. This suggests that the vortex sheet, at least on the thicker wings, may collapse into a part of the wing upper surface as the incidence falls to zero, rather than shrink into the leading edge in a uniform manner. The negative curvature of the sheet near the leading edge for $a = 0{\cdot}6$ in Fig. 9b has already been mentioned. At lower values of a the curvature near the edge is positive, as on thinner wings, but for $a = 0{\cdot}2$ two points of inflexion appear further along the sheet. To pursue these mathematically interesting trends to lower values of a would require a different approach to the definition of the sheet shape. as the calculated shape in the transformed plane is becoming parallel to the radius vectors from the position of the isolated vortex, i.e. $d\bar{r}/d\vartheta$ in Fig. 3 is becoming large.

The positions calculated for the isolated vortex are summarized in Fig. 10a. The full lines represent the sequences of calculated solutions, the broken lines are interpolations between them. The figure puts into perspective the points of detail discussed above and emphasizes the magnitude of the changes introduced by thickness. These are much larger at the larger incidences, on a scale apparently related to the size of the vortex itself. Further minor oddities of the solution appear for very thick wings. Fig. 10b is taken from Ref. 19 with a trivial change in the abscissa. It shows the measured variation in the position of the vortex centre, interpreted as the point of minimum total head, in a plane 45 per cent of the length of the wing from the apex, in a low-speed wind tunnel in conditions where the secondary separation was laminar. The variations with thickness and incidence shown in Figs. 10a and b are clearly of the same type: inboard and upward as the incidence increases, outboard and upward as the thickness increases for thin wings and outboard and downward as the thickness increases for thick wings.

The actual differences between measurement and calculation are shown in Figs. 11a for the lateral position and 11b for the height. Experimental points from Ref. 14 for a wing with apex angle 20 degrees and leading-edge angle, δ, of 30 degrees have now been added. Russell determined the vortex core position in two ways, as the minimum of total head, and as the point where the local velocity vector was directed through the apex of the wing. The difference between the determinations was generally small and the mean of the two has been plotted. There appears to be a small discrepancy between the measurements of Refs. 14 and 19, tentatively attributed by Russell to a slight yaw of the model to the flow, but it is not enough to affect the present discussion. For the wings with $\delta = 30$ degrees, the difference in lateral position between calculation and experiment is about the same as that found in Ref. 1 between the calculations for a flat plate and the measurements on thin wings with laminar secondary separation. The error remains

about the same for $\delta = 60$ and 90 degrees, but seems a little larger for $\delta = 120$ degrees, though the measurements on this wing were made at larger values of a. For the height, the error at $\delta = 30$ degrees is small, about the same as that attributed to different definitions of the vortex centre in Ref. 1. As the thickness increases the discrepancy grows, until at $\delta = 120$ degrees it is as large as the discrepancy in lateral position.

It seems almost certain that these discrepancies are to be attributed to the presence of the secondary separation between the peak suction on the wing and the leading edge. On the positive side, it is known that a change in the state of the secondary boundary layer produces a measurable shift in the position of the vortex. On the negative side, three alternative explanations can be rejected. First, the effect of different identifications of the vortex centre was shown to be small in Ref. 1. Second, the wing thickness is properly represented in these calculations. Third, the effect of the assumption of slenderness can be dismissed; since this assumption should become more valid as the Mach number increases towards one, whereas the pressure measurements of Ref. 22 point to a slight inboard movement of the vortex, so increasing the observed discrepancy, as the Mach number increases subsonically.

4.2. *Circulation.*

In Tables 2–9 the circulation, Γ, about the isolated vortex and the circulation, Γ_s, about the finite part of the vortex sheet represented in the calculations, are tabulated in nondimensional form. Since the choice of the extent of the finite part of the sheet is essentially arbitrary, the overall circulation about the leading-edge vortex, $\Gamma + \Gamma_s$, is a more significant quantity.

Fig. 12 shows how the overall circulation varies with incidence for two thick wings and the flat plate. It is clear that the growth of circulation with incidence becomes increasingly non-linear as the thickness increases; so that, although at $a = 0{\cdot}2$ an increase of edge angle from 0 to 60 degrees more than halves the circulation, at $a = 2{\cdot}0$ the corresponding reduction is less than 15 per cent. The calculations terminate tantalizingly short of the origin, but it seems likely that the initial rate of growth of circulation at zero incidence is zero for the thick wings and non-zero for the flat plate.

Some measurements of circulation made by Kirkpatrick[20] on two rhombic cones with edge angles of 60 degrees are shown for comparison. The measurements were made by traversing a five-tube yawmeter, aligned with the local flow, round a contour 'enclosing' the vortex, in a plane 45 per cent of the length of the wing from the apex, in a low-speed wind tunnel. The tangential component of the velocity so found was integrated round the contour. Practical difficulties prevented a very close approach to the wing, so that part of the shear layer from the leading edge was left outside the contour. Further, part of the secondary vortex, whose circulation is of the opposite sense, may have lain within the contour. The measurements must therefore under-estimate the circulation of the primary vortex and Kirkpatrick[20] is inclined to identify the result with the total circulation of the primary and secondary vortices, rather than with that of the primary vortex represented in the calculations. In these circumstances the relation between the results of the calculation and the experiment shown in Fig. 12 is very satisfactory.

Further experimental points, obtained in the same way at various lengthwise stations over the forward half of rhombic cones at two values of a, are compared with the present calculations in Fig. 13. The vertical extent of the symbols indicates the spread of the measurements for different traversing contours. Again the measurements fall below the calculation in a manner consistent with the nature of the comparison.

Figs. 12 and 13, showing how the circulation about the vortex falls as the thickness increases, suggest that the circulation may be correlated with the size of the vortex. There is no obvious measure of the latter, but a typical length is the distance of the isolated vortex (or the core of the real vortex) from the leading edge. In Fig. 14, the overall circulation is plotted against this distance, $((1-y)^2+z^2)^{\frac{1}{2}}$, for five values of a spanning the present calculations, with δ running from 0 to 120 degrees along each curve. In spite of the irregularities in the shapes of the individual curves, a roughly consistent variation of circulation with scale emerges. The experimental points, based on results of Refs. 19 and 20 for $\delta = 30$, 60 and 90 degrees, show that the corresponding correlation in the real flow (if it exists) is different.

The density of the circulation along the finite part of the vortex sheet (or the 'strength' of the sheet) is shown in Fig. 15 for $a = 1$ and five values of δ. For the flat plate, the form of the variation is familiar from Ref. 1, though the finite part of the sheet is not long enough in the present calculations for the characteristic

waviness to appear. As the thickness increases, the strength of the sheet is reduced, in parallel with the reduction in overall circulation. The sheet also shrinks in length with the reduction in size of the vortex. Thus Γ_s, the circulation on the sheet falls more rapidly than the overall circulation, as can be seen in Table 8. The shape of the curves near $\sigma=0$ in Fig. 15 is not definitely established by the present calculations. For $\delta=30$ and 120 degrees the calculated points are shown, and they are sufficient to indicate that the initial rapid decrease in strength found for the flat plate is much reduced for the thicker wings.

4.3. *Normal Force.*

In Tables 2–9, the normal force coefficient, C_N, divided by K^2 to produce a quantity depending on δ and a only, is listed. Since this quantity increases more than proportionately with a, a more revealing display is obtained by dividing it by a, to give $C_N/\alpha K$. The latter is plotted in Fig. 16 against a for five values of δ. Experimental measurements are shown for comparison. Those of Fink and Taylor[28] are obtained by integrating the pressures measured at a forward station on a delta wing of apex angle 20 degrees formed from a thin plate with chamfered leading edges. Those of Kirkpatrick[18] are obtained from strain-gauge measurements of the normal force on the forward halves of split models in the form of rhombic cones of aspect ratio 0·8 ($\delta=30$, 60 and 90 degrees) and 0·462 ($\delta=120$ degrees). The experimental results therefore correspond closely to conical flow conditions, as postulated in the theory.

The calculated curves for $a>0$ have been joined to the values of $C_N/\alpha K$ given by slender body theory for attached flow at $a=0$, i.e. by the first term of (B.7):

$$\frac{C_N}{\alpha K}=4\left(\frac{\pi\varepsilon d^2}{s^2}-\cot\varepsilon\pi\right), \tag{52}$$

where s/d is given by (8). Some smoothing of the experimental results at low values of a has been taken over from Ref. 18.

Any lifting surface theory for thin wings in attached flow would provide only a single value for the function plotted in Fig. 16, slender thin-wing theory for instance yielding 2π, the limit of (52) as $\varepsilon\to 0{\cdot}5$. The reduction in lift due to the thickness of these slender wings in attached flow is shown by the intercepts of the calculated curves at $a=0$. The effect of leading-edge separation is shown by the rise of the curves away from these intercepts as a increases. It is clear that thickness affects the non-linear element in the lift much more than the linear part. For instance, for a wing of aspect ratio 1 at 15 degrees incidence, the calculated non-linear lift is 42 per cent of the total for a flat plate, but only 21 per cent of the total for a wing with $\delta=90$ degrees, i.e. its thickness equal to its span.

The experimental measurements lie somewhat below the calculated results, throughout. For the rhombic cones, the discrepancy increases as the thickness increases. On the 'flat-plate' wing, the chamfered surfaces cover most of the wing ahead of the measuring station, so the measurements are likely to correspond to the calculated solution for a value of δ equal to the angle between the chamfered surfaces, viz. 8·75 degrees, rather than to $\delta=0$. On this basis, they, too, are consistent with a discrepancy which increases as the thickness increases, as shown in Fig. 17. On the thicker wings, the discrepancy also increases with incidence, but for the flat plate and $\delta=30$ degrees it is little affected by incidence. In all cases there appears to be a residual disagreement in the slope of the normal force, $dC_N/d\alpha$, at zero incidence, found by Kirkpatrick[18] to be around 5 per cent. The present model of the separated flow cannot hope to be more accurate than the basic representation of the attached flow and Fig. 16 indicates that it is not very much worse.

The larger discrepancies found for the thicker wings can be associated with the corresponding discrepancies in vortex position, attributed in 4.1 to the influence of the secondary separation. This agrees with Rott's observation[17] of the importance of secondary separation on thick wedges in unsteady flow.

5. *Conclusions.*

It has been shown that the method of Ref. 1 for calculating the effects of leading-edge separation on slender wings in conical flow can be extended without difficulty to deal with thick wings. Comparison

with experiment shows a small reduction in the accuracy to which vortex position and normal force can be predicted as the thickness increases. These results tend to confirm that it is the omission of secondary separation from the model that causes the discrepancy between calculation and measurements made in nearly conical subsonic flow.

The calculations confirm the observed trends:

(a) for the non-linear lift to be more reduced by thickness than is the linear component of the lift;

(b) for increasing thickness to move the centre of the leading-edge vortex outboard in an arc, first upwards and then, for the thicker wings, downwards; and

(c) for increasing thickness to reduce the circulation and size of the vortex.

They also show further details of the shape and strength of the vortex sheet, in particular that:

(d) the vortex sheet springs from the leading edge in a direction tangential to the lower surface of the wing, and

(e) the strength of the sheet is reduced by increasing thickness in a similar way to the overall circulation.

Acknowledgement.

The help of Mrs. M. G. Joyce in guiding the calculations through Mercury and ATLAS is gratefully acknowledged.

LIST OF SYMBOLS

a	$=\alpha/K$, incidence parameter
a'	Size of step in search procedure
A_j	*See* equation (26)
b	Angle in ζ-plane (Fig. 3)
b_j	Value of r/s at point of vortex sheet
$b_0(x)$	Spatial influence function of slender-body theory
B_j	*See* equation (40)
c	Residual error in normal velocity condition
c_j	Value of θ at point of vortex sheet
C_N	Coefficient of normal force
d	Semi-span of transform of wing in ζ-plane
d_j	Value of $\bar{r}/(d)$ at point of vortex sheet
e_{2j}	Value of $(d\bar{\sigma}/d\vartheta)/(d)$ at intermediate point
e_{2j-1}	Value of $(d\bar{r}/d\vartheta)/(d)$ at intermediate point
e'	Tolerance on change in g
f_{2j}	Value of $d\theta/d\vartheta$ at intermediate point
f_{2j-1}	Value of $(dr/d\vartheta)/s$ at intermediate point
f'	Tolerance on $\lvert F\rvert$
F	Complex number proportional to force on vortex and cut
${}_2F_1$	Hypergeometric function
g	$=\Gamma/KU(d)$
g_j	Value of $(d\Delta\Phi/d\vartheta)/KU(d)$ at pivotal point
g'	Tolerance on $\{\delta_j\}$
h_j	Value of ϑ at pivotal point on sheet
h'	Discriminator on $\{\delta_j\}$
k	Number of pivotal points adjusted when vortex is moved
K	Cotangent of angle of sweep of wing leading edge
M	Mach number
n	Inward normal to sheet, also number of pivotal points
r	Polar coordinate of sheet in cross-flow plane
$\bar{r}$	Polar coordinate of sheet in ζ-plane
$\mathscr{R}$	Real part
s	Local semi-span of wing

S	Local cross-sectional area of slender body
U	Speed of undisturbed stream
v_n	Normal component of velocity on sheet in ζ-plane
v_{t_m}	Mean tangential component of velocity on sheet in ζ-plane
W	Complex potential
W_1	Complex potential of the attached flow
x, y, z	Rectangular cartesian coordinates in the wing
y, z	Coordinates of vortex in cross-flow plane, referred to s
y_j, z_j	Coordinates of point on sheet in cross-flow plane, referred to s
$\bar{y}, \bar{z}$	Coordinates of vortex in ζ-plane, referred to d
$\bar{y}_j, \bar{z}_j$	Coordinates of point on sheet in ζ-plane, referred to d
Z	Complex variable in cross-flow plane
α	Incidence of wing
β	$=(1-M^2)^{\frac{1}{2}}$
B	$=(M^2-1)^{\frac{1}{2}}$
$B(x, y)$	Beta function
γ_k	*See* above equation (23)
Γ	Circulation of starboard isolated vortex
$\Gamma(z)$	Gamma function
Γ_s	Circulation about finite part of sheet
δ	Angle included between wing surfaces
δ_k	Increment in d_{2k}, *see* Fig. 4. Also used in equation (23)
Δ	Difference operator across sheet
ε	$=\frac{1}{2}(1-\delta/2\pi)$
ε_j	*See* equation (34)
ζ	Complex variable in transformed plane
ζ_j	y_j+iz_j
θ	Polar coordinate of sheet in cross-flow plane
$\theta_1\ \theta_2\ \theta_3$	Angles in ζ-plane, *see* Fig. 2a
ϑ	Polar coordinate of sheet in ζ-plane
λ_j	Value of $(d\Delta\Phi/d\vartheta)/KU(d)$ at intermediate point
μ_j, ν_j	*See* equation (38)
σ	Arc length along sheet in cross-flow plane
$\bar{\sigma}$	Arc length along sheet in ζ-plane
φ	Angle between tangent and radius vector (Fig. 1)
Φ	Lifting part of disturbance potential
χ_j	Angle of rotation of tangent in ζ-plane

REFERENCES

No.	Author(s)	Title, etc.
1	J. H. B. Smith	Improved calculations of leading-edge separation from slender delta wings. RAE Technical Report 66070 (ARC 27897) (1966). *Proc. Roy. Soc. A., 306*, 67-90 (1968).
2	E. C. Polhamus	A concept of the vortex lift of sharp-edge delta wings, based on a leading-edge-suction analogy. NASA TN D-3767, December 1966.
3	S. D. Ermolenko	On the non-linear theory of wings of small aspect ratio. *Izv. Vysshikh Uchebnykh Zavedenii (ser. Av. Tekh.) 2*, 9-18 (1966). RAE Library Translation 1218 (1967).
4	S. M. Belotserkovskii	Calculation of the flow about wings of arbitrary planform at a wide range of angles of attack. *Mek. Zh. Gaz. 4*, 32-44 (1968). RAE Library Translation 1433 (1970).
5	R. K. Nangia and G. L. Hancock	A theoretical investigation for delta wings with leading-edge separation at low speeds. A.R.C. CP 1086 (1968).
6	C. E. Brown and W. H. Michael	On slender delta wings with leading-edge separation. NACA Tech. Note 3430, April 1955. Also: *J. Aero. Sci., 21*, 690-694 and 706 (1954).
7	K. Gersten	Nichtlineare Tragflächentheorie inbesondere für Tragflügel mit kleinem Seitenverhältnis. *Ingenieur-Archiv, 30*, 431-452 (1961).
8	H. C. Garner and D. E. Lehrian	Non-linear theory of steady forces on wings with leading-edge flow separation. A.R.C. R. & M. 3375 (1963).
9	A. H. Sacks, R. E. Lundberg and C. W. Hanson	A theoretical investigation of the aerodynamics of slender wing-body combinations exhibiting leading-edge separation. NASA CR-719, March 1967.
10	E. S. Levinsky	Non-linear lift and pressure distribution on slender conical bodies with strakes at low speeds. NASA CR-1202, October 1968.
11	E. S. Levinsky, M. H. Y. Wei and R. L. Maki	Theoretical studies of vortex flow on slender wing-body combinations. *in* Analytical methods in aircraft aerodynamics. NASA SP-228, October 1969.
12	J. H. B. Smith	A theory of the separated flow from the curved leading edge of a slender wing. A.R.C. R. & M. 3116 (1957).

REFERENCES—*continued*

No.	*Author(s)*	*Title, etc.*
13	C. E. Jobe	An aerodynamic theory of slender wings with leading-edge separation. Unpublished thesis, Ohio State University (1966).
14	H. Portnoy and S. C. Russell..	The effect of small conical thickness distributions on the separated flow past slender delta wings. A.R.C. CP 1189 (1971).
15	E. C. Maskell	Similarity laws governing the initial growth of leading-edge vortex sheets in conical flow past sharp-edged slender bodies. *Tenth Int. Congr. Appl. Mech.*, Stresa (1960).
16	D. L. I. Kirkpatrick	Experiments on the similarity of leading-edge vortices above slender wings in subsonic conical flow. RAE Technical Report 66288 (1966). Also: Jahrbuch 1967 WGLR, 223-231.
17	N. Rott	Diffraction of a weak shock with vortex generation. *J. Fluid Mech., 1*, 111-128 (1956).
18	D. L. I. Kirkpatrick	Investigation of the normal force characteristics of slender delta wings with various rhombic cross-sections in subsonic conical flow. A.R.C. CP 922 (1965).
19	D. L. I. Kirkpatrick and J. D. Field ..	Experimental investigation of the positions of the leading-edge vortices above slender delta wings with various rhombic cross-sections in subsonic conical flow. A.R.C. CP 925 (1966).
20	D. L. I. Kirkpatrick	A study of the leading-edge vortices above slender wings. Thesis: University of Southampton (1970).
21	J. W. Britton	Pressure measurements at supersonic speeds on three uncambered conical wings of unit aspect ratio. A.R.C. CP 641 (1962).
22	J. H. B. Smith and A. G. Kurn	Pressure measurements on a slender rhombic cone at incidence at Mach numbers from 0·4 to 1·1. A.R.C. R. & M. 3626 (1968).
23	L. A. Wyatt and L. F. East ..	Low-speed measurements of skin-friction on a slender wing. A.R.C. R. & M. 3499 (1966).
24	G. N. Ward	Linearised theory of steady high-speed flow. Cambridge University Press (1955).
25	I. S. Gradshteyn and I. M. Ryzhik	Table of integrals, series and products. (Fourth ed. translated into English) Academic Press (1965).

REFERENCES—*continued*

No.	*Author(s)*	*Title, etc.*
26		Specification for data processing problem definition and analysis. Part 1. Flow chart symbols. BS 4058: Part 1 : 1966, British Standards Institution.
27	K. W. Mangler and J. H. B. Smith	Behaviour of the vortex sheet at the trailing edge of a lifting wing. RAE Technical Report 69049 (A.R.C. 32061) (1969). *Aeronautical Journal, 74*, 906-8, November 1970.
28	P. T. Fink and J. Taylor	Some early experiments on vortex separation. A.R.C. R. & M. 3489 (1957).

APPENDIX I

Equations for Innermost Iteration.

Since the only quantities which alter in the course of this iteration are g and $\{g_j\}$, it is advantageous to work with the unchanging coefficients of these quantities. This Appendix gives these coefficients.

At the jth intermediate point let

$$\frac{d\zeta}{d\bar{\sigma}} = \alpha_j + i\beta_j , \tag{A.1}$$

where α_j and β_j follow from equation (31). Also let the term in $\frac{1}{KU}\frac{dW}{d\zeta}$, as given by (32), which is independent of g and $\{g_j\}$ be expressed as $v_j - iw_j$. Then, by (30), we can write

$$\frac{v_{t_m}}{KU} = \delta_{j,0} g + \sum_{k=1}^{n} \delta_{j,k} g_k + \delta_{j,n+1} \tag{A.2}$$

at the jth intermediate point, where

$$\left.\begin{aligned}
\delta_{j,0} &= \frac{\bar{y}}{\pi} \frac{2\alpha_j \bar{y}_{2j-1}(\bar{z} - \bar{z}_{2j-1}) + \beta_j(\bar{y}_{2j-1}^2 - \bar{y}^2 - (\bar{z}_{2j-1} - \bar{z})^2)}{((\bar{y}_{2j-1} - \bar{y})^2 + (\bar{z}_{2j-1} - \bar{z})^2)((\bar{y}_{2j-1} + \bar{y})^2 + (\bar{z}_{2j-1} - \bar{z})^2)}, \\
\delta_{j,k} &= \frac{\bar{y}_{2k}(h_{k+1} - h_{k-1})}{2\pi} \times \\
&\quad \times \frac{2\alpha_j \bar{y}_{2j-1}(\bar{z}_{2k} - \bar{z}_{2j-1}) + \beta_j(\bar{y}_{2j-1}^2 - \bar{y}_{2k}^2 - (\bar{z}_{2j-1} - \bar{z}_{2k})^2)}{((\bar{y}_{2j-1} - \bar{y}_{2k})^2 + (\bar{z}_{2j-1} - \bar{z}_{2k})^2)((\bar{y}_{2j-1} + \bar{y}_{2k})^2 + (\bar{z}_{2j-1} - \bar{z}_{2k})^2)}
\end{aligned}\right\} \tag{A.3}$$

and

$$\delta_{j,n+1} = \alpha_j v_j + \beta_j w_j .$$

Hence, by (34) and (38), we can write

$$\mu_j = \delta'_{j,0} g + \sum_{k=1}^{n} \delta'_{j,k} g_k + \delta'_{j,n+1} , \tag{A.4}$$

where

$$\left.\begin{aligned}
\delta'_{j,0} &= \tau_j \delta_{j,0} , \\
\delta'_{j,k} &= \tau_j \delta_{j,k}
\end{aligned}\right\} \tag{A.5}$$

and

$$\delta'_{j,n+1} = \tau_j \left(\delta_{j,n+1} - \frac{b_{2j-1} s f_{2j-1}}{e_{2j}} \right) - h_{j+1} + h_{j-1}$$

where

$$\tau_j=\frac{4s}{e_{2j}}\left|\frac{1+(\bar{y}_{2j-1}+i\bar{z}_{2j-1})^2}{(\bar{y}_{2j-1}+i\bar{z}_{2j-1})^2}\right|^{2\varepsilon}. \tag{A.6}$$

Note that $h_{n+1}=2h_n-h_{n-1}$ in these relations. The development along these lines cannot be carried further, since the B_j in equation (40) are no longer linear functions of g and $\{g_j\}$. From (38) and (39) we can write

$$\left.\begin{aligned} B_j&=4\left(\frac{h_j-h_{j-1}}{h_{j+1}-h_{j-1}}+\frac{h_{j+1}-h_j}{h_{j+1}-h_{j-1}}\frac{\mu_{j+1}+\nu_{j+1}}{\mu_j}\right)\frac{(\mu_n+\nu_n)(\mu_{n-1}+\nu_{n-1})\ldots(\mu_{j+2}+\nu_{j+2})}{\mu_n\mu_{n-1}\ldots\mu_{j+1}}\\ &\text{for } j=1,2,\ldots n-1 \text{ and}\\ B_n&=\frac{4}{\mu_n}\left(\frac{h_{n+1}-h_{n-2}}{h_n-h_{n-2}}-\frac{h_n-h_{n-1}}{h_n-h_{n-2}}\frac{\mu_n+\nu_n}{\mu_{n-1}}\right). \end{aligned}\right\} \tag{A.7}$$

The procedure is to compute and store the $n(n+2)$ numbers $\delta'_{j,k}, j=1,2,\ldots n, k=0,1,\ldots(n+1)$; the $n-1$ numbers ν_j given by (38); and $n+1$ numbers

$$D_0=\frac{2\bar{y}}{\bar{y}^2+\bar{z}^2} \text{ and } D_j=\frac{A_j\bar{y}_{2j}}{\bar{y}_{2j}^2+\bar{z}_{2j}^2} \quad j=1,2,\ldots n,$$

before entering the innermost iteration. Then, for an approximate set of g and $\{g_j\}$, the μ_j follow from (A.4), the B_j follow from (A.7) and the next approximation to g follows from equation (41), written as

$$g\left(D_0+\sum_{j=1}^{n}D_jB_j\right)=2\pi a. \tag{A.8}$$

The corresponding approximation to the g_j follows from equation (40).

In this way the innermost iteration can be performed very quickly, in spite of the complication of the expressions involved.

APPENDIX II

Calculation of the Lift or Normal Force.

The lift acting on a slender body is given by Ward in equation 9.7.11 of Ref. 25. He uses axes aligned with the free stream, $0x'y'z'$, related to the present system by

$$x' = x\cos\alpha + z\sin\alpha\,,$$

$$y' = y$$

and

$$z' = -x\sin\alpha + z\cos\alpha\,.$$

Then, if $Z' = y' + iz'$, and $Z'_g(x')$ is the value of Z' at the centre of area of the cross-section of the body by the plane $x' = \text{const.}$, the complex lateral force is given by

$$F = \rho U^2\left[2\pi b + \frac{d}{dx'}(Z'_g(x')S(x'))\right], \tag{B.1}$$

where b is the coefficient of Z'^{-1} in the expansion of W/U for large Z' and $S(x')$ is the area of the cross-section of the body by the plane $x' = \text{const.}$

For the small incidences of the present approximation,

$$Z' = y' + iz' = y + i(-x\alpha + z) = Z - i\alpha x\,,$$

and, since $Z_g = 0$, $Z'_g = -i\alpha x$. Again for small incidence and thickness, $S(x') = S(x) = 2K^2x^2\cot\varepsilon\pi$, and differentiation with respect to x and x' are equivalent, so that

$$\frac{d}{dx'}(Z'_g(x')S(x')) = \frac{d}{dx}(-2iK^2\alpha x^3\cot\varepsilon\pi) = -6i\alpha s^2\cot\varepsilon\pi\,. \tag{B.2}$$

To evaluate b it is convenient to deal separately with the contribution b_1 from the complex potential W_1 of the attached flow, and with the remainder, b_2, from the representation of the leading-edge vortices. We can find b_1 exactly. We first need the expansion of ζ in terms of Z' for large Z'. From equation (7)

$$\frac{dZ}{d\zeta} = \left(\frac{\zeta^2}{\zeta^2 + d^2}\right)^{\varepsilon} = 1 - \frac{\varepsilon d^2}{\zeta^2} + \ldots\,,$$

therefore

$$Z = \zeta + \text{const} + \frac{\varepsilon d^2}{\zeta} + \ldots\,.$$

The real part of the constant of integration must vanish because ζ large and imaginary corresponds to Z imaginary, and its imaginary part must vanish because $Z(\bar{\zeta}) = \overline{Z(\zeta)}$. Hence

$$\zeta = Z - \frac{\varepsilon d^2}{Z} + \ldots = Z' + i\alpha x - \frac{\varepsilon d^2}{Z'} + \ldots\,. \tag{B.3}$$

Now, from equation (10)

$$\frac{dW_1}{d\zeta} = -i\alpha U + \frac{KU\cos\varepsilon\pi}{i\pi}\int_{-id}^{id}\left|\left(\frac{t^2}{t^2+d^2}\right)^{\varepsilon}\right|\frac{dt}{\zeta - t}$$

$$= -i\alpha U + \frac{KU\cos\varepsilon\pi}{\pi}\int_{-d}^{d}\left(\frac{t^2}{d^2-t^2}\right)^{\varepsilon}\frac{dt}{\zeta-it},$$

and so

$$\frac{W_1}{U} = -i\alpha\zeta + \frac{K\cos\varepsilon\pi}{\pi}\int_{-d}^{d}\left(\frac{t^2}{d^2-t^2}\right)^{\varepsilon} ln\,(\zeta-it)dt + \text{const}$$

$$= -i\alpha\zeta + \frac{K\cos\varepsilon\pi}{\pi}\,ln\,\zeta\int_{-d}^{d}\left(\frac{t^2}{d^2-t^2}\right)^{\varepsilon}dt - \frac{iK\cos\varepsilon\pi}{\pi\zeta}\int_{-d}^{d}\left(\frac{t^2}{d^2-t^2}\right)^{\varepsilon}tdt + \text{const} + 0(\zeta^{-2}).$$

Now the first of these integrals is $2s$ cosec $\varepsilon\pi$, by equation (8), and the second vanishes, so that

$$\frac{W_1}{U} = -i\alpha\zeta + \frac{2Ks\cot\varepsilon\pi}{\pi}\,ln\,\zeta + \text{const} + 0(\zeta^{-2})$$

$$= -i\alpha\left(Z' + i\alpha x - \frac{\varepsilon d^2}{Z'}\right) + \frac{2Ks\cot\varepsilon\pi}{\pi}\left(ln\,Z' + \frac{i\alpha x}{Z'}\right) + \text{const} + 0(Z'^{-2}).$$

Therefore

$$b_1 = i\alpha\left(\varepsilon d^2 + \frac{2s^2\cot\varepsilon\pi}{\pi}\right). \tag{B.4}$$

We now find b_2 in terms of the numerical approximation to the vortices. From (10) it is clear that the leading term in the expansion of W for large ζ is $0(\zeta^{-1})$, so only this term need be considered. To this order ζ, Z and Z' are equal. The appropriate expression can therefore be written down by inspection of equations (10) and (24):

$$b_2 = -\frac{\Gamma(\zeta_V+\bar{\zeta}_V)}{2\pi iU} - \frac{Kd^2}{2\pi i}\sum_{j=1}^{n} g_j\bar{y}_{2j}(h_{j+1}-h_{j-1})$$

$$= \frac{iKg\bar{y}d^2}{\pi} + \frac{iKd^2}{2\pi}\sum_{j=1}^{n} g_j\bar{y}_{2j}(h_{j+1}-h_{j-1}) \tag{B.5}$$

with $h_0=0$ and $h_{n+1}=h_n$ by convention. Suitable factors d^2 have been reintroduced where necessary to restore proper dimensionality.

The lift is the imaginary part of the complex force F and follows from (B.1), (B.2), (B.4) and (B.5):

$$L = \rho U^2\left[2\pi\alpha\varepsilon d^2 - 2\alpha s^2\cot\varepsilon\pi + 2Kg\bar{y}d^2 + Kd^2\sum_{j=1}^{n} g_j\bar{y}_{2j}(h_{j+1}-h_{j-1})\right]. \tag{B.6}$$

Since the wing area is xs or s^2/K, and lift and normal force are the same in this approximation, we have

$$\frac{C_N}{K^2}=4a\left(\frac{\pi\varepsilon d^2}{s^2}-\cot\varepsilon\pi\right)+\frac{4g\bar{y}d^2}{s^2}+\frac{2d^2}{s^2}\sum_{j=1}^{n}g_j\bar{y}_{2j}(h_{j+1}-h_{j-1})\,. \tag{B.7}$$

When $\varepsilon=\frac{1}{2}$, $d=s$, and this agrees with equation (63) of Ref. 1. The first term represents the linear lift arising in attached flow.

APPENDIX III

The Velocity Near the Leading Edge in Attached Flow.

Although the formulation (9) of the velocity in the attached flow past the rhombic cone is suitable for numerical evaluation at points away from the wing surface, numerical difficulties would arise from the treatment of the Cauchy principal-value integral which occurs on the surface itself. Moreover, the formulation reveals nothing of the analytic behaviour of the velocity field near the leading edge, where $\zeta=0$. In this Appendix alternative expressions are derived from (9) to complement it in these respects. Equation (C.9) was used as a check that the numerical treatment of (9), embodied in equation (23), was in fact adequate for the present calculations.

Using W_1 for the complex potential of the attached flow, we can write equation (9) as

$$\frac{1}{KU}\frac{dW_1}{d\zeta}=-ia+\frac{\cos\varepsilon\pi}{\pi i}\int_{-id}^{id}\left|\left(\frac{t^2}{t^2+d^2}\right)^{\varepsilon}\right|\frac{dt}{\zeta-t}$$

$$=-ia+\frac{\cos\varepsilon\pi}{\pi}\int_{-\frac{\pi}{2}}^{\frac{\pi}{2}}\frac{|\tan^{2\varepsilon}\theta|\cos\theta\,d\theta}{\zeta_1-i\sin\theta}$$

(where $t=id\sin\theta$ and $\zeta=\zeta_1 d$)

$$=-ia+I\frac{\cos\varepsilon\pi}{\pi}, \tag{C.1}$$

where

$$I=2\zeta_1\int_0^{\frac{\pi}{2}}\frac{\tan^{2\varepsilon}\theta\cos\theta\,d\theta}{\zeta_1^2+\sin^2\theta}. \tag{C.2}$$

By differentiation we find

$$\frac{dI}{d\zeta_1}=-\frac{I}{\zeta_1}+2\int_0^{\frac{\pi}{2}}\tan^{2\varepsilon}\theta\sin\theta\frac{2\sin\theta\cos\theta}{(\zeta_1^2+\sin^2\theta)^2}d\theta.$$

Integration by parts gives

$$\frac{dI}{d\zeta_1}=-\frac{I}{\zeta_1}+\frac{2}{\zeta_1^2+1}\int_0^{\frac{\pi}{2}}\frac{\tan^{2\varepsilon}\theta\cos\theta\,(2\varepsilon+\cos^2\theta)d\theta}{\zeta_1^2+\sin^2\theta},$$

and this can be rearranged as

$$\frac{dI}{d\zeta_1}-\frac{2\varepsilon}{\zeta_1(\zeta_1^2+1)}I=-\frac{2}{\zeta_1^2+1}J, \tag{C.3}$$

where $J=\int_0^{\frac{\pi}{2}} \tan^{2\varepsilon}\theta\cos\theta\,d\theta=\frac{1}{2}B(\frac{1}{2}+\varepsilon,1-\varepsilon)$,

by setting $x=\tan^2\theta$ and using 3.194.3 of Ref. 25. The solution of the differential equation (C.3) can be written at once as

$$\left(\frac{\zeta_1^2+1}{\zeta_1^2}\right)^{\varepsilon} I=2J\int_{\zeta_1}^{\infty}\frac{dt}{t^{2\varepsilon}(t^2+1)^{1-\varepsilon}},\ \text{since } I\to 0 \text{ as } \zeta_1\to\infty\,.$$

Again using section 3.194 of Ref. 25 we can express the integral in terms of the beta function and the hypergeometric function:

$$I=\left(\frac{\zeta_1^2}{\zeta_1^2+1}\right)^{\varepsilon} B(\tfrac{1}{2}+\varepsilon,1-\varepsilon)\left\{\tfrac{1}{2}B(\tfrac{1}{2}-\varepsilon,\tfrac{1}{2})-\frac{\zeta_1^{1-2\varepsilon}}{1-2\varepsilon}\,{}_2F_1\left(1-\varepsilon,\tfrac{1}{2}-\varepsilon;\frac{3}{2}-\varepsilon,-\zeta_1^2\right)\right\}. \tag{C.4}$$

The product of the beta functions simplifies, using the definition in terms of the gamma function and equation 8.334.2 of Ref. 25:

$$B(\tfrac{1}{2}+\varepsilon,1-\varepsilon)B(\tfrac{1}{2}-\varepsilon,\tfrac{1}{2})=2\pi/\cos\pi\varepsilon\,. \tag{C.5}$$

To display the analytic behaviour of the velocity near the leading edge we need the expansion of the hypergeometric function:

$${}_2F_1(\alpha,\beta;\gamma,z)=1+\frac{\alpha\beta}{\gamma 1}z+\frac{\alpha(\alpha+1)\beta(\beta+1)}{\gamma(\gamma+1).1.2}z^2+\ldots\,. \tag{C.6}$$

Then, remembering

$$\frac{dZ}{d\zeta}=\left(\frac{\zeta^2}{\zeta^2+d^2}\right)^{\varepsilon}=\left(\frac{\zeta_1^2}{\zeta_1^2+1}\right)^{\varepsilon} \tag{C.7}$$

we have, by (C.1), (C.4), (C.5), (C.6) and (C.7)

$$\frac{1}{KU}\frac{dW_1}{dZ}=-ia\left(\frac{\zeta_1^2+1}{\zeta_1^2}\right)^{\varepsilon}+1-\frac{\cos\varepsilon\pi}{\pi}B(\tfrac{1}{2}+\varepsilon,1-\varepsilon)\frac{\zeta_1^{1-2\varepsilon}}{1-2\varepsilon}(1-(1-2\varepsilon)O(\zeta_1^2))\,.$$

The first term on the right is the incidence-dependent velocity. If ζ_1 is real, corresponding to Z in the plane of the wing and ahead of the leading edge, this is an upwash which tends to infinity at the leading edge like $\zeta_1^{-2\varepsilon}$, i.e. like $(Z-s)^{-2\varepsilon/(1+2\varepsilon)}$. If ζ_1 is imaginary, corresponding to Z on the wing surface, the incidence term is tangential to the wing surface, according to the interpretation of the conformal transformation in Section 2. The remaining terms on the right give the velocity at zero incidence and this is clearly non-singular. Provided $\varepsilon<\frac{1}{2}$, i.e. the wing has thickness, the lateral velocity increases towards KU as the leading edge is approached from upstream (ζ_1 real and small). In the limit $\varepsilon\to\frac{1}{2}$, the velocity field at zero incidence vanishes.

$$= -i\alpha U + \frac{KU\cos\varepsilon\pi}{\pi}\int_{-d}^{d}\left(\frac{t^2}{d^2-t^2}\right)^{\varepsilon}\frac{dt}{\zeta-it},$$

and so

$$\frac{W_1}{U} = -i\alpha\zeta + \frac{K\cos\varepsilon\pi}{\pi}\int_{-d}^{d}\left(\frac{t^2}{d^2-t^2}\right)^{\varepsilon} ln\,(\zeta-it)dt + \text{const}$$

$$= -i\alpha\zeta + \frac{K\cos\varepsilon\pi}{\pi} ln\,\zeta \int_{-d}^{d}\left(\frac{t^2}{d^2-t^2}\right)^{\varepsilon}dt - \frac{iK\cos\varepsilon\pi}{\pi\zeta}\int_{-d}^{d}\left(\frac{t^2}{d^2-t^2}\right)^{\varepsilon}tdt + \text{const} + 0(\zeta^{-2}).$$

Now the first of these integrals is $2s\,\text{cosec}\,\varepsilon\pi$, by equation (8), and the second vanishes, so that

$$\frac{W_1}{U} = -i\alpha\zeta + \frac{2Ks\cot\varepsilon\pi}{\pi} ln\,\zeta + \text{const} + 0(\zeta^{-2})$$

$$= -i\alpha\left(Z' + i\alpha x - \frac{\varepsilon d^2}{Z'}\right) + \frac{2Ks\cot\varepsilon\pi}{\pi}\left(ln\,Z' + \frac{i\alpha x}{Z'}\right) + \text{const} + 0(Z'^{-2}).$$

Therefore

$$b_1 = i\alpha\left(\varepsilon d^2 + \frac{2s^2\cot\varepsilon\pi}{\pi}\right). \tag{B.4}$$

We now find b_2 in terms of the numerical approximation to the vortices. From (10) it is clear that the leading term in the expansion of W for large ζ is $0(\zeta^{-1})$, so only this term need be considered. To this order ζ, Z and Z' are equal. The appropriate expression can therefore be written down by inspection of equations (10) and (24):

$$b_2 = -\frac{\Gamma(\zeta_V+\bar{\zeta}_V)}{2\pi iU} - \frac{Kd^2}{2\pi i}\sum_{j=1}^{n} g_j\bar{y}_{2j}(h_{j+1}-h_{j-1})$$

$$= \frac{iKg\bar{y}d^2}{\pi} + \frac{iKd^2}{2\pi}\sum_{j=1}^{n} g_j\bar{y}_{2j}(h_{j+1}-h_{j-1}) \tag{B.5}$$

with $h_0=0$ and $h_{n+1}=h_n$ by convention. Suitable factors d^2 have been reintroduced where necessary to restore proper dimensionality.

The lift is the imaginary part of the complex force F and follows from (B.1), (B.2), (B.4) and (B.5):

$$L = \rho U^2\left[2\pi\alpha\varepsilon d^2 - 2\alpha s^2\cot\varepsilon\pi + 2Kg\bar{y}d^2 + Kd^2\sum_{j=1}^{n} g_j\bar{y}_{2j}(h_{j+1}-h_{j-1})\right]. \tag{B.6}$$

Since the wing area is xs or s^2/K, and lift and normal force are the same in this approximation, we have

$$\frac{C_N}{K^2}=4a\left(\frac{\pi\varepsilon d^2}{s^2}-\cot\varepsilon\pi\right)+\frac{4g\bar{y}d^2}{s^2}+\frac{2d^2}{s^2}\sum_{j=1}^{n}g_j\bar{y}_{2j}(h_{j+1}-h_{j-1})\,. \tag{B.7}$$

When $\varepsilon=\frac{1}{2}$, $d=s$, and this agrees with equation (63) of Ref. 1. The first term represents the linear lift arising in attached flow.

APPENDIX III

The Velocity Near the Leading Edge in Attached Flow.

Although the formulation (9) of the velocity in the attached flow past the rhombic cone is suitable for numerical evaluation at points away from the wing surface, numerical difficulties would arise from the treatment of the Cauchy principal-value integral which occurs on the surface itself. Moreover, the formulation reveals nothing of the analytic behaviour of the velocity field near the leading edge, where $\zeta=0$. In this Appendix alternative expressions are derived from (9) to complement it in these respects. Equation (C.9) was used as a check that the numerical treatment of (9), embodied in equation (23), was in fact adequate for the present calculations.

Using W_1 for the complex potential of the attached flow, we can write equation (9) as

$$\frac{1}{KU}\frac{dW_1}{d\zeta}=-ia+\frac{\cos\varepsilon\pi}{\pi i}\int_{-id}^{id}\left|\left(\frac{t^2}{t^2+d^2}\right)^{\varepsilon}\right|\frac{dt}{\zeta-t}$$

$$=-ia+\frac{\cos\varepsilon\pi}{\pi}\int_{-\frac{\pi}{2}}^{\frac{\pi}{2}}\frac{|\tan^{2\varepsilon}\theta|\cos\theta\,d\theta}{\zeta_1-i\sin\theta}$$

(where $t=id\sin\theta$ and $\zeta=\zeta_1 d$)

$$=-ia+I\frac{\cos\varepsilon\pi}{\pi}, \tag{C.1}$$

where

$$I=2\zeta_1\int_0^{\frac{\pi}{2}}\frac{\tan^{2\varepsilon}\theta\cos\theta\,d\theta}{\zeta_1^2+\sin^2\theta}. \tag{C.2}$$

By differentiation we find

$$\frac{dI}{d\zeta_1}=-\frac{I}{\zeta_1}+2\int_0^{\frac{\pi}{2}}\tan^{2\varepsilon}\theta\sin\theta\frac{2\sin\theta\cos\theta}{(\zeta_1^2+\sin^2\theta)^2}d\theta.$$

Integration by parts gives

$$\frac{dI}{d\zeta_1}=-\frac{I}{\zeta_1}+\frac{2}{\zeta_1^2+1}\int_0^{\frac{\pi}{2}}\frac{\tan^{2\varepsilon}\theta\cos\theta\,(2\varepsilon+\cos^2\theta)d\theta}{\zeta_1^2+\sin^2\theta},$$

and this can be rearranged as

$$\frac{dI}{d\zeta_1}-\frac{2\varepsilon}{\zeta_1(\zeta_1^2+1)}I=-\frac{2}{\zeta_1^2+1}J, \tag{C.3}$$

where $J=\int_0^{\frac{\pi}{2}} \tan^{2\varepsilon}\theta\cos\theta\,d\theta=\frac{1}{2}B(\frac{1}{2}+\varepsilon,1-\varepsilon)$,

by setting $x=\tan^2\theta$ and using 3.194.3 of Ref. 25. The solution of the differential equation (C.3) can be written at once as

$$\left(\frac{\zeta_1^2+1}{\zeta_1^2}\right)^{\varepsilon} I=2J\int_{\zeta_1}^{\infty}\frac{dt}{t^{2\varepsilon}(t^2+1)^{1-\varepsilon}},\ \text{since } I\to 0 \text{ as } \zeta_1\to\infty\,.$$

Again using section 3.194 of Ref. 25 we can express the integral in terms of the beta function and the hypergeometric function:

$$I=\left(\frac{\zeta_1^2}{\zeta_1^2+1}\right)^{\varepsilon}B(\tfrac{1}{2}+\varepsilon,1-\varepsilon)\left\{\tfrac{1}{2}B(\tfrac{1}{2}-\varepsilon,\tfrac{1}{2})-\frac{\zeta_1^{1-2\varepsilon}}{1-2\varepsilon}\,{}_2F_1\left(1-\varepsilon,\tfrac{1}{2}-\varepsilon;\frac{3}{2}-\varepsilon,-\zeta_1^2\right)\right\}. \tag{C.4}$$

The product of the beta functions simplifies, using the definition in terms of the gamma function and equation 8.334.2 of Ref. 25:

$$B(\tfrac{1}{2}+\varepsilon,1-\varepsilon)B(\tfrac{1}{2}-\varepsilon,\tfrac{1}{2})=2\pi/\cos\pi\varepsilon\,. \tag{C.5}$$

To display the analytic behaviour of the velocity near the leading edge we need the expansion of the hypergeometric function:

$${}_2F_1(\alpha,\beta;\gamma,z)=1+\frac{\alpha\beta}{\gamma 1}z+\frac{\alpha(\alpha+1)\beta(\beta+1)}{\gamma(\gamma+1).1.2}z^2+\ldots\,. \tag{C.6}$$

Then, remembering

$$\frac{dZ}{d\zeta}=\left(\frac{\zeta^2}{\zeta^2+d^2}\right)^{\varepsilon}=\left(\frac{\zeta_1^2}{\zeta_1^2+1}\right)^{\varepsilon} \tag{C.7}$$

we have, by (C.1), (C.4), (C.5), (C.6) and (C.7)

$$\frac{1}{KU}\frac{dW_1}{dZ}=-ia\left(\frac{\zeta_1^2+1}{\zeta_1^2}\right)^{\varepsilon}+1-\frac{\cos\varepsilon\pi}{\pi}B(\tfrac{1}{2}+\varepsilon,1-\varepsilon)\frac{\zeta_1^{1-2\varepsilon}}{1-2\varepsilon}(1-(1-2\varepsilon)O(\zeta_1^2))\,.$$

The first term on the right is the incidence-dependent velocity. If ζ_1 is real, corresponding to Z in the plane of the wing and ahead of the leading edge, this is an upwash which tends to infinity at the leading edge like $\zeta_1^{-2\varepsilon}$, i.e. like $(Z-s)^{-2\varepsilon/(1+2\varepsilon)}$. If ζ_1 is imaginary, corresponding to Z on the wing surface, the incidence term is tangential to the wing surface, according to the interpretation of the conformal transformation in Section 2. The remaining terms on the right give the velocity at zero incidence and this is clearly non-singular. Provided $\varepsilon<\frac{1}{2}$, i.e. the wing has thickness, the lateral velocity increases towards KU as the leading edge is approached from upstream (ζ_1 real and small). In the limit $\varepsilon\to\frac{1}{2}$, the velocity field at zero incidence vanishes.

For numerical calculation it is convenient to write

$$ {}_2F_1\left(1-\varepsilon, \tfrac{1}{2}-\varepsilon; \frac{3}{2}-\varepsilon, -\zeta_1^2\right) = \frac{(\zeta_1^2+1)^\varepsilon}{B(\frac{1}{2}, 1-\varepsilon)} \int_0^1 \frac{dt}{t^{\frac{1}{2}}(1-t)^\varepsilon(1+\zeta_1^2 t)}, \tag{C.8} $$

by 9.131.1 and 9.111 of Ref. 25. Then, by (C.1), (C.4), (C.5) and (C.8)

$$ \frac{1}{KU}\frac{dW_1}{d\zeta} = -ia + \left(\frac{\zeta_1^2}{\zeta_1^2+1}\right)^\varepsilon - \frac{2\zeta_1}{\pi} \int_0^{\frac{\pi}{2}} \frac{\cos^{1-2\varepsilon}\theta d\theta}{1+\zeta_1^2 \sin^2\theta}, \tag{C.9} $$

where $t = \sin^2\theta$ has been introduced into (C.8). This form is suitable for numerical evaluation for small values of ζ_1 and for points on the wing surface if these are required.

TABLE 2

Solutions for $\varepsilon = 0{\cdot}5$, $\delta = 0$.

a	y	z	$\frac{\Gamma}{KUs}$	$\frac{\Gamma_s}{KUs}$	$\frac{C_N}{K^2}$
0·2	0·910	0·047	0·676	0·080	1·573
0·3	0·874	0·071	1·025	0·160	2·511
0·4	0·841	0·096	1·378	0·263	3·542
0·5	0·815	0·121	1·730	0·376	4·645
0·6	0·788	0·147	2·089	0·508	5·832
0·7	0·764	0·172	2·457	0·649	7·090
0·8	0·743	0·198	2·835	0·795	8·414
0·9	0·725	0·222	3·227	0·941	9·800
1·0	0·709	0·247	3·633	1·096	11·25
1·1	0·696	0·270	4·059	1·246	12·76
1·2	0·686	0·291	4·501	1·394	14·31
1·3	0·676	0·312	4·960	1·542	15·92
1·4	0·669	0·332	5·440	1·690	17·59
1·5	0·663	0·350	5·936	1·835	19·30
1·6	0·658	0·368	6·450	1·974	21·06
1·7	0·654	0·385	6·981	2·110	22·86
1·8	0·652	0·400	7·527	2·239	24·70
1·9	0·649	0·415	8·091	2·374	26·60
2·0	0·648	0·429	8·662	2·499	28·51
2·1	0·647	0·443	9·252	2·622	30·48
2·2	0·646	0·456	9·856	2·744	32·48
2·3	0·646	0·469	10·48	2·865	34·53
2·4	0·646	0·481	11·06	2·981	36·60
2·5	0·646	0·492	11·74	3·092	38·71
2·6	0·647	0·503	12·39	3·207	40·87
2·7	0·648	0·514	13·05	3·311	43·04
2·8	0·648	0·524	13·72	3·419	45·25

TABLE 3

Solutions for $\varepsilon = \frac{5}{12}(0{\cdot}4167)$, $\delta = 30°$

a	y	z	$\frac{\Gamma}{KUs}$	$\frac{\Gamma_s}{KUs}$	$\frac{C_N}{K^2}$
0·1	0·977	0·022	0·184	0·010	0·618
0·2	0·949	0·050	0·463	0·046	1·341
0·3	0·926	0·077	0·764	0·099	2·152
0·4	0·904	0·104	1·087	0·172	3·055
0·5	0·882	0·131	1·424	0·260	4·043
0·6	0·861	0·159	1·772	0·364	5·117
0·7	0·840	0·187	2·132	0·485	6·273
0·8	0·821	0·215	2·499	0·613	7·503
0·9	0·802	0·244	2·876	0·755	8·813
1·0	0·784	0·273	3·265	0·906	10·20
1·1	0·769	0·300	3·666	1·059	11·64
1·2	0·754	0·328	4·080	1·222	13·16
1·3	0·740	0·354	4·510	1·385	14·73
1·4	0·728	0·380	4·952	1·553	16·36
1·5	0·718	0·404	5·415	1·717	18·05
1·6	0·709	0·426	5·890	1·877	19·77
1·7	0·701	0·448	6·386	2·041	21·56
1·8	0·695	0·468	6·901	2·199	23·39
1·9	0·690	0·486	7·431	2·353	25·26
2·0	0·686	0·504	7·969	2·503	27·16
2·1	0·682	0·521	8·533	2·657	29·14
2·2	0·680	0·537	9·110	2·797	31·13
2·3	0·677	0·552	9·695	2·946	33·17
2·4	0·676	0·566	10·30	3·082	35·24
2·5	0·675	0·579	10·91	3·215	37·35
2·6	0·674	0·592	11·55	3·354	39·52
2·7	0·674	0·604	12·19	3·479	41·68

TABLE 4

Solutions for $\varepsilon = \frac{4}{12}$ (0·3333), $\delta = 60°$

a	y	z	$\frac{\Gamma}{KUs}$	$\frac{\Gamma_s}{KUs}$	$\frac{C_N}{K^2}$
0·1	0·989	0·020	0·107	0·006	0·544
0·2	0·974	0·048	0·314	0·028	1·160
0·3	0·960	0·074	0·556	0·064	1·847
0·4	0·947	0·099	0·827	0·112	2·605
0·5	0·934	0·126	1·123	0·172	3·439
0·6	0·922	0·152	1·440	0·244	4·347
0·7	0·909	0·179	1·775	0·327	5·333
0·8	0·896	0·206	2·125	0·422	6·394
0·9	0·883	0·233	2·489	0·528	7·535
1·0	0·870	0·261	2·866	0·645	8·753
1·1	0·858	0·289	3·254	0·772	10·04
1·2	0·845	0·318	3·654	0·910	11·42
1·3	0·833	0·347	4·063	1·057	12·86
1·4	0·820	0·376	4·484	1·214	14·38
1·5	0·809	0·404	4·918	1·373	15·96
1·6	0·797	0·433	5·360	1·545	17·62
1·7	0·787	0·461	5·818	1·715	19·33
1·8	0·776	0·489	6·283	1·896	21·11
1·9	0·767	0·515	6·768	2·077	22·94
2·0	0·758	0·540	7·266	2·257	24·82
2·1	0·751	0·565	7·777	2·437	26·76
2·2	0·744	0·588	8·306	2·615	28·73

TABLE 5

Solutions for $\varepsilon = \frac{3}{12}(0{\cdot}25)$, $\delta = 90°$

a	y	z	$\frac{\Gamma}{KUs}$	$\frac{\Gamma_s}{KUs}$	$\frac{C_N}{K^2}$
0·1	0·990	0·028	0·082	0·008	0·491
0·2	0·990	0·043	0·202	0·018	1·013
0·3	0·984	0·066	0·381	0·040	1·586
0·4	0·978	0·089	0·588	0·070	2·203
0·5	0·972	0·112	0·822	0·108	2·872
0·6	0·966	0·134	1·081	0·153	3·593
0·7	0·960	0·157	1·361	0·204	4·370
0·8	0·954	0·180	1·661	0·264	5·205
0·9	0·948	0·203	1·982	0·331	6·102
1·0	0·942	0·226	2·318	0·404	7·053
1·1	0·936	0·250	2·672	0·484	8·072
1·2	0·930	0·273	3·040	0·570	9·148
1·3	0·924	0·296	3·422	0·664	10·29
1·4	0·918	0·320	3·820	0·766	11·50
1·5	0·912	0·344	4·231	0·874	12·78
1·6	0·906	0·369	4·654	0·990	14·12
1·7	0·899	0·393	5·088	1·111	15·53
1·8	0·893	0·418	5·536	1·243	17·02
1·9	0·886	0·444	5·993	1·385	18·58
2·0	0·880	0·469	6·463	1·525	20·19
2·1	0·873	0·496	6·943	1·681	21·89
2·2	0·866	0·522	7·431	1·844	23·66

TABLE 6

Solutions for $\varepsilon = \frac{2}{12}$ (0·1667), $\delta = 120^{c}$

a	y	z	$\frac{\Gamma}{KUs}$	$\frac{\Gamma_s}{KUs}$	$\frac{C_N}{K^2}$
0·2	0·983	0·068	0·139	0·026	0·899
0·3	0·993	0·071	0·250	0·034	1·379
0·4	0·996	0·077	0·375	0·043	1·869
0·5	0·998	0·089	0·529	0·059	2·387
0·6	0·996	0·110	0·722	0·088	2·951
0·7	0·995	0·127	0·922	0·115	3·529
0·8	0·994	0·143	1·134	0·144	4·130
0·9	0·993	0·160	1·367	0·179	4·765
1·0	0·991	0·178	1·619	0·217	5·437
1·1	0·990	0·194	1·885	0·258	6·138
1·2	0·989	0·211	2·166	0·301	6·874
1·3	0·988	0·228	2·466	0·349	7·653
1·4	0·987	0·245	2·780	0·400	8·468
1·5	0·986	0·261	3·107	0·454	9·329
1·6	0·985	0·278	3·450	0·510	10·21
1·7	0·984	0·294	3·806	0·570	11·15
1·8	0·983	0·311	4·179	0·634	12·13
1·9	0·982	0·327	4·561	0·699	13·14
2·0	0·981	0·344	4·957	0·768	14·20
2·1	0·980	0·362	5·374	0·845	15·33
2·2	0·978	0·379	5·798	0·924	16·50

TABLE 7

Solutions for $a = 0{\cdot}5$

ε	y	z	$\frac{\Gamma}{KUs}$	$\frac{\Gamma_s}{KUs}$	$\frac{C_N}{K^2}$
0·12	1·000	0·121	0·440	0·080	2·227
0·14	0·999	0·098	0·470	0·063	2·282
0·16	0·998	0·088	0·508	0·057	2·354
0·18	0·993	0·099	0·590	0·073	2·476
0·20	0·988	0·101	0·651	0·080	2·576
0·22	0·981	0·107	0·722	0·092	2·695
0·24	0·975	0·109	0·786	0·102	2·809
0·26	0·967	0·116	0·863	0·118	2·945
0·28	0·960	0·117	0·929	0·128	3·066
0·30	0·950	0·122	1·005	0·146	3·210
0·32	0·941	0·124	1·075	0·160	3·345
0·34	0·931	0·127	1·148	0·179	3·489
0·36	0·920	0·128	1·218	0·196	3·628
0·38	0·906	0·131	1·293	0·220	3·779
0·40	0·894	0·131	1·363	0·240	3·921
0·42	0·880	0·131	1·435	0·264	4·068
0·44	0·865	0·130	1·507	0·289	4·212
0·46	0·848	0·128	1·581	0·318	4·359
0·48	0·831	0·125	1·654	0·347	4·504

TABLE 8

Solutions for $a = 1{\cdot}0$

ε	y	z	$\frac{\Gamma}{KUs}$	$\frac{\Gamma_s}{KUs}$	$\frac{C_N}{K^2}$
0·12	1·010	0·138	1·195	0·128	4·687
0·14	1·003	0·158	1·380	0·166	4·996
0·16	0·994	0·173	1·558	0·203	5·319
0·18	0·985	0·186	1·736	0·243	5·674
0·20	0·974	0·199	1·911	0·285	6·050
0·22	0·962	0·212	2·083	0·333	6·451
0·24	0·949	0·221	2·240	0·378	6·848
0·26	0·935	0·231	2·393	0·429	7·259
0·28	0·919	0·240	2·534	0·482	7·668
0·30	0·902	0·249	2·668	0·542	8·084
0·32	0·883	0·257	2·790	0·605	8·491
0·34	0·864	0·263	2·903	0·664	8·876
0·36	0·843	0·269	3·005	0·732	9·256
0·38	0·823	0·271	3·103	0·791	9·603
0·40	0·802	0·273	3·191	0·856	9·939
0·42	0·781	0·273	3·278	0·915	10·25
0·44	0·761	0·269	3·366	0·967	10·53
0·46	0·742	0·264	3·451	1·017	10·79
0·48	0·725	0·256	3·540	1·060	11·03

TABLE 9

Solutions for $a = 1{\cdot}5$

ε	y	z	$\frac{\Gamma}{KUs}$	$\frac{\Gamma_s}{KUs}$	$\frac{C_N}{K^2}$
0·12	1·012	0·202	2·308	0·261	7·636
0·14	1·002	0·228	2·660	0·339	8·311
0·16	0·990	0·253	2·999	0·424	9·058
0·18	0·976	0·277	3·322	0·516	9·861
0·20	0·960	0·297	3·611	0·608	10·67
0·22	0·942	0·317	3·880	0·711	11·52
0·24	0·923	0·335	4·119	0·816	12·35
0·26	0·901	0·353	4·334	0·931	13·19
0·28	0·877	0·369	4·522	1·049	14·00
0·30	0·852	0·385	4·686	1·174	14·78
0·32	0·826	0·398	4·831	1·299	15·52
0·34	0·800	0·407	4·958	1·413	16·17
0·36	0·776	0·412	5·080	1·512	16·76
0·38	0·754	0·412	5·200	1·595	17·26
0·40	0·733	0·409	5·316	1·668	17·72
0·42	0·715	0·403	5·435	1·725	18·11
0·44	0·699	0·393	5·552	1·770	18·45
0·46	0·685	0·380	5·678	1·800	18·77
0·48	0·674	0·366	5·807	1·816	19·04

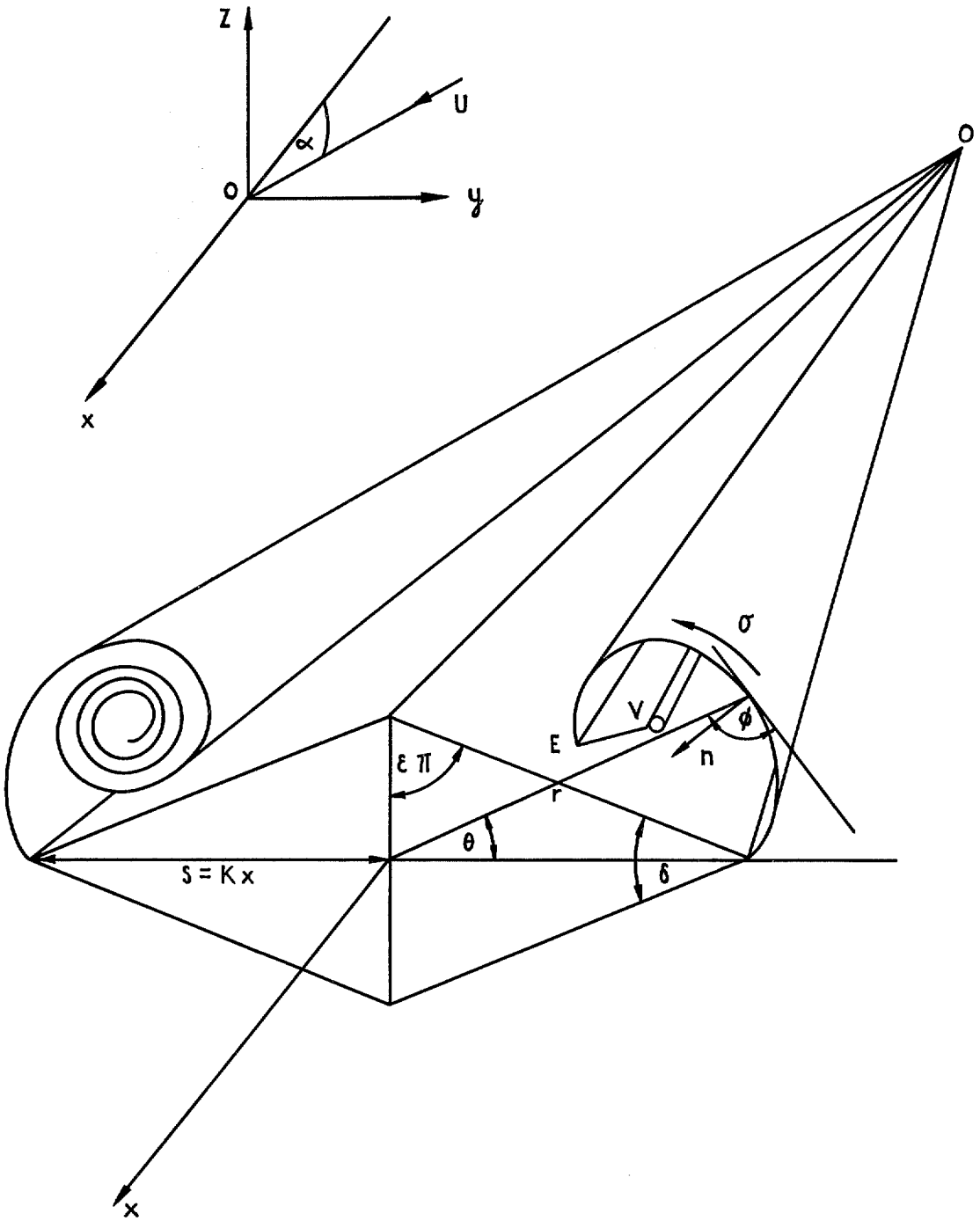

FIG. 1. Wing and coordinate system.

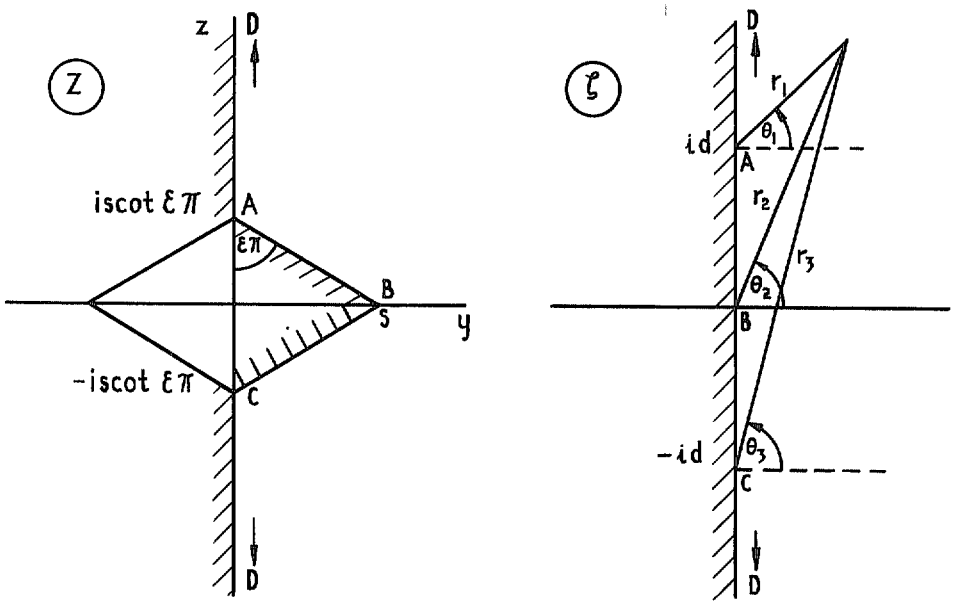

FIG. 2a. Conformal transformation.

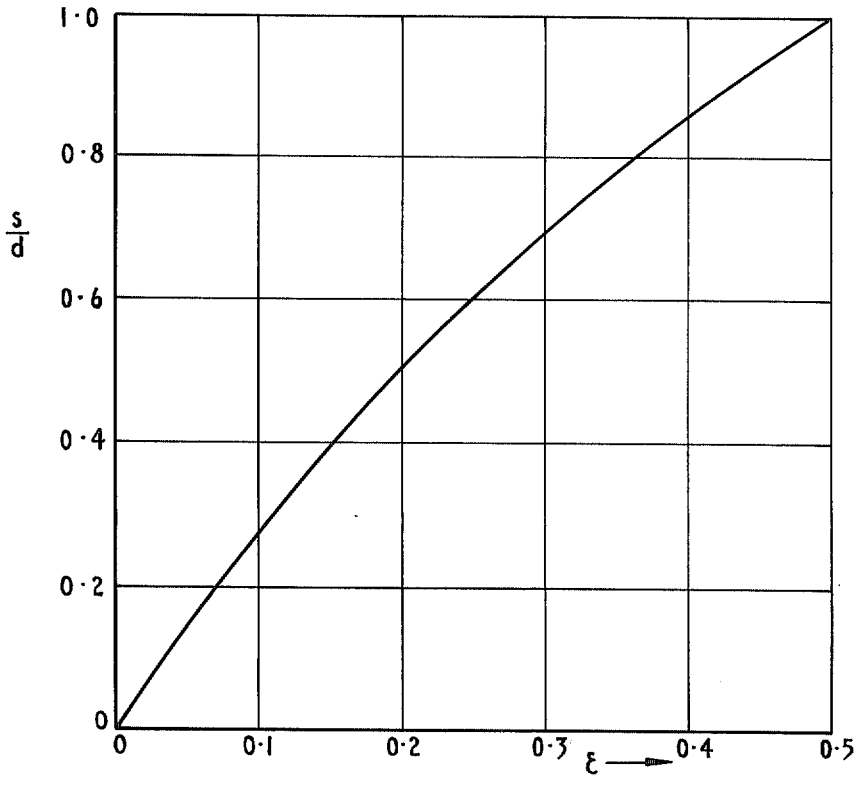

FIG. 2b. Variation of transformation parameter with thickness of wing.

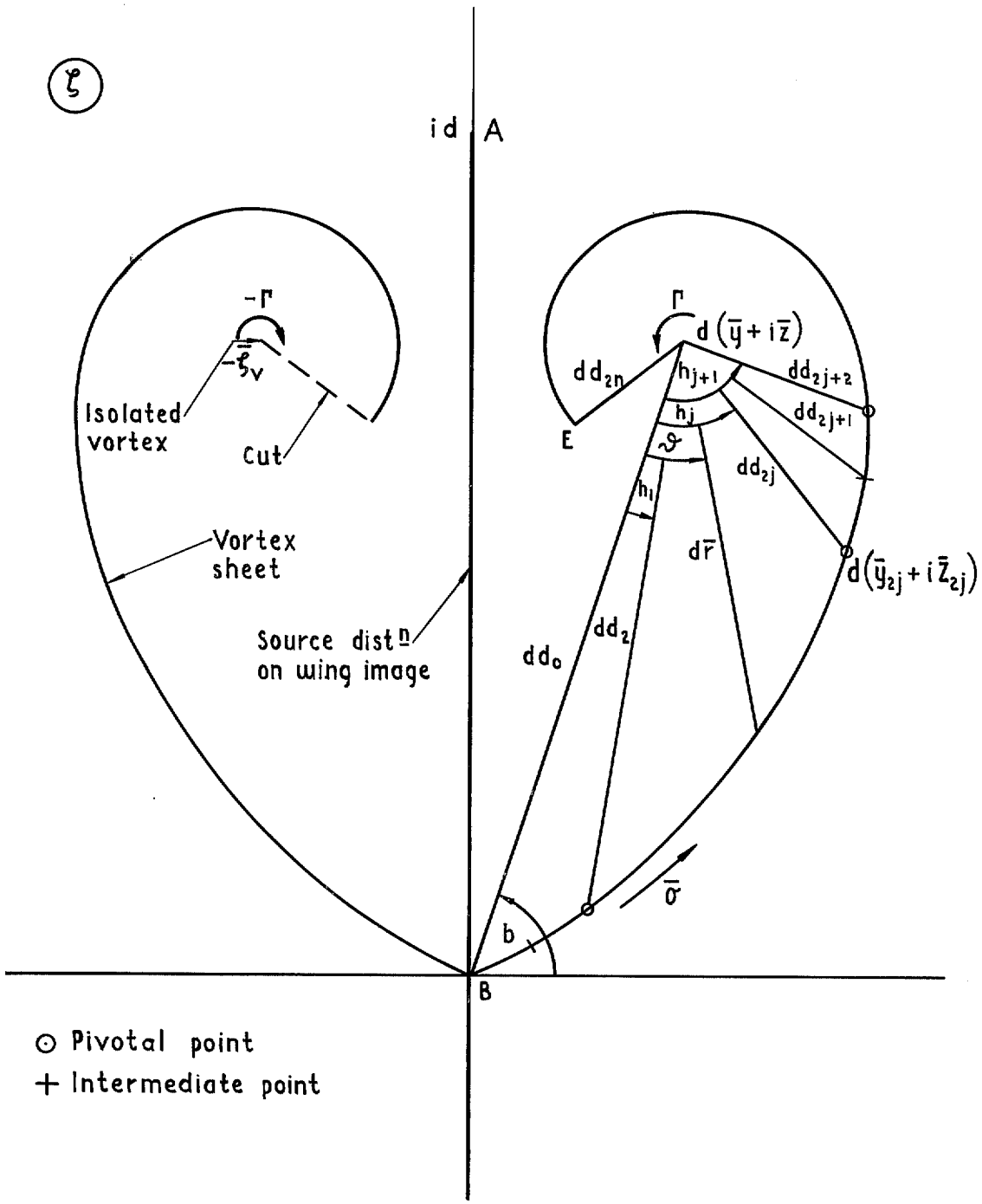

FIG. 3. Configuration in transformed plane.

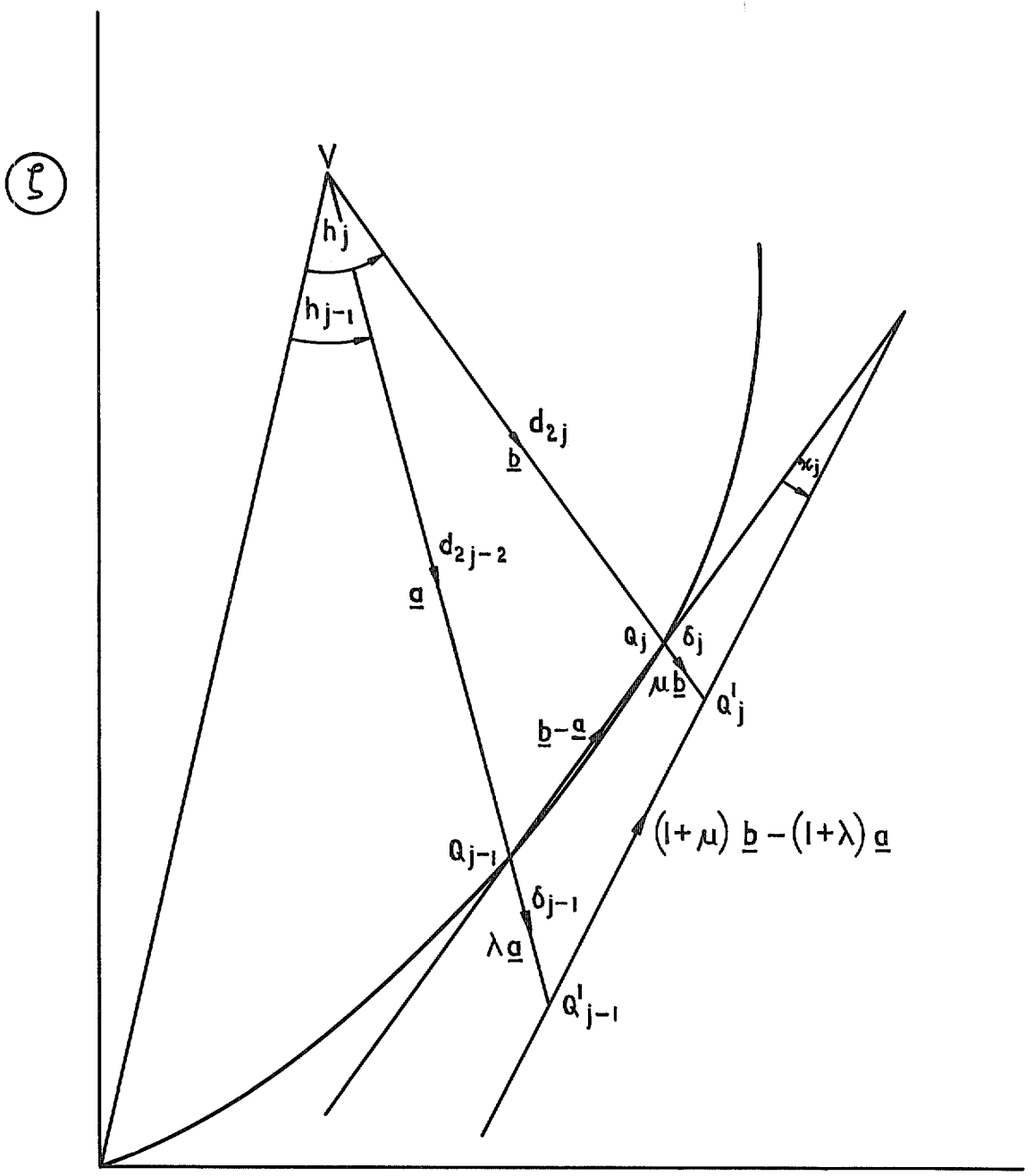

FIG. 4. Application of normal velocity condition.

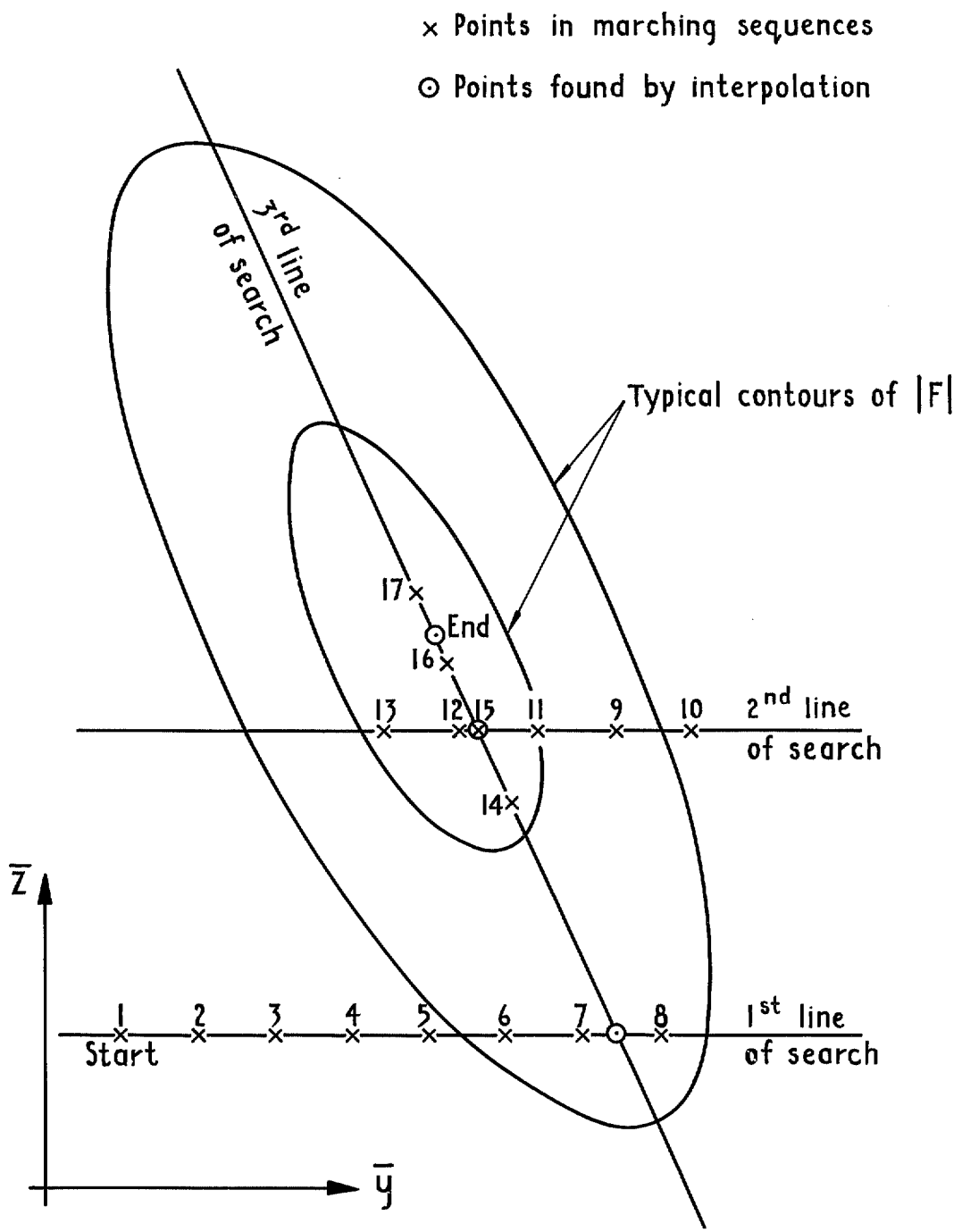

FIG. 5. Search procedure for minimum of $|F(\bar{y}, \bar{z})|$

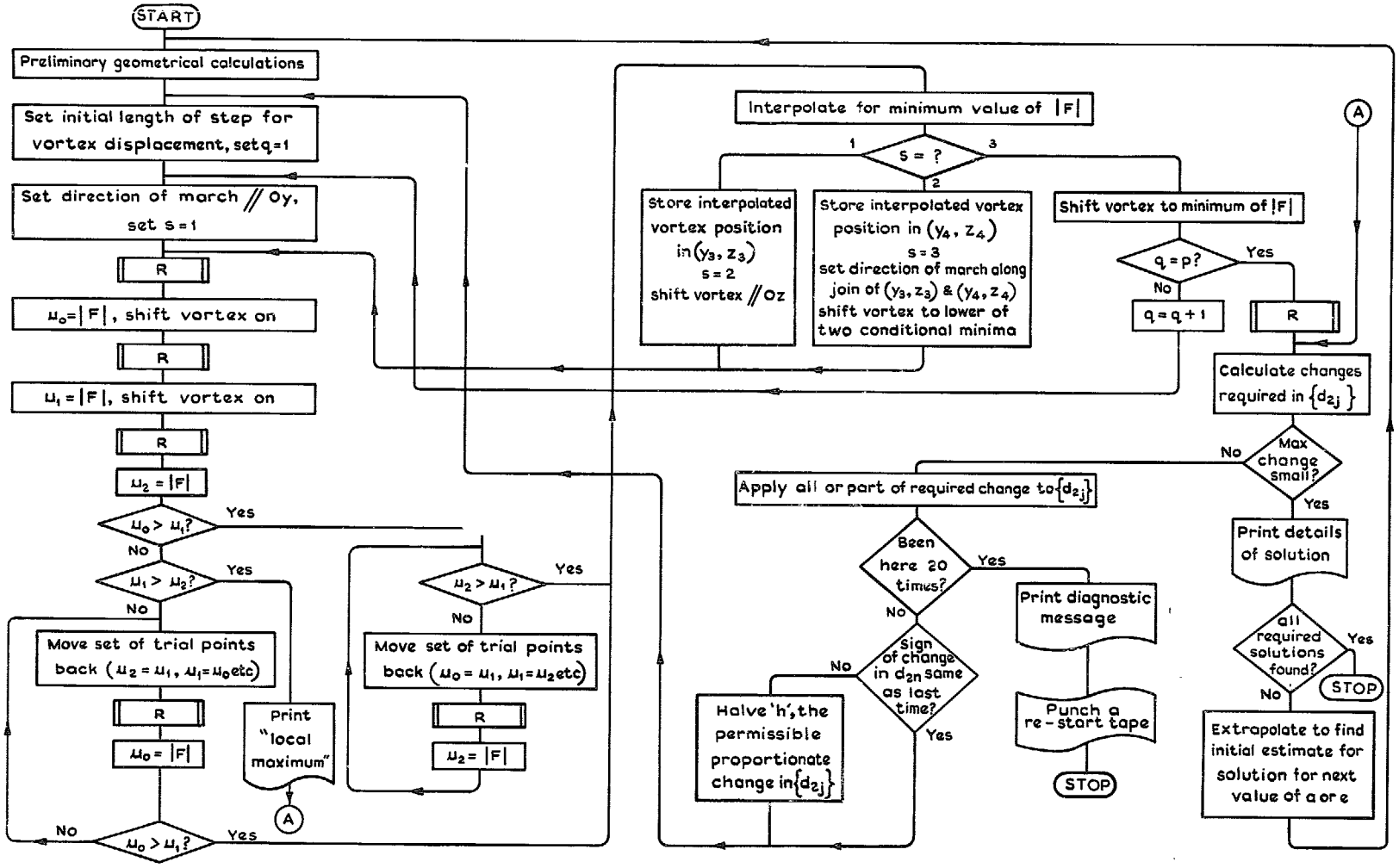

FIG. 6. Flow diagram of computer program.

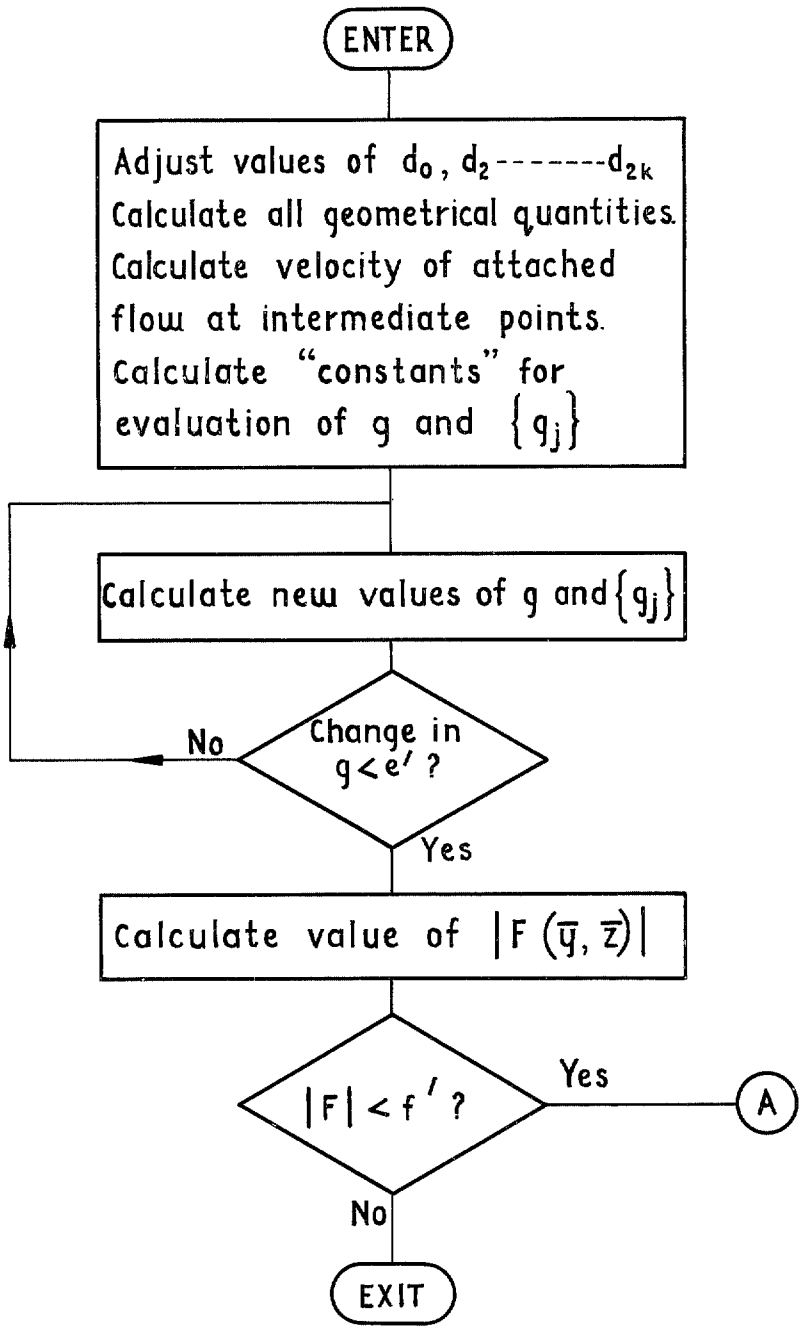

FIG. 7. Flow diagram of subroutine *R*.

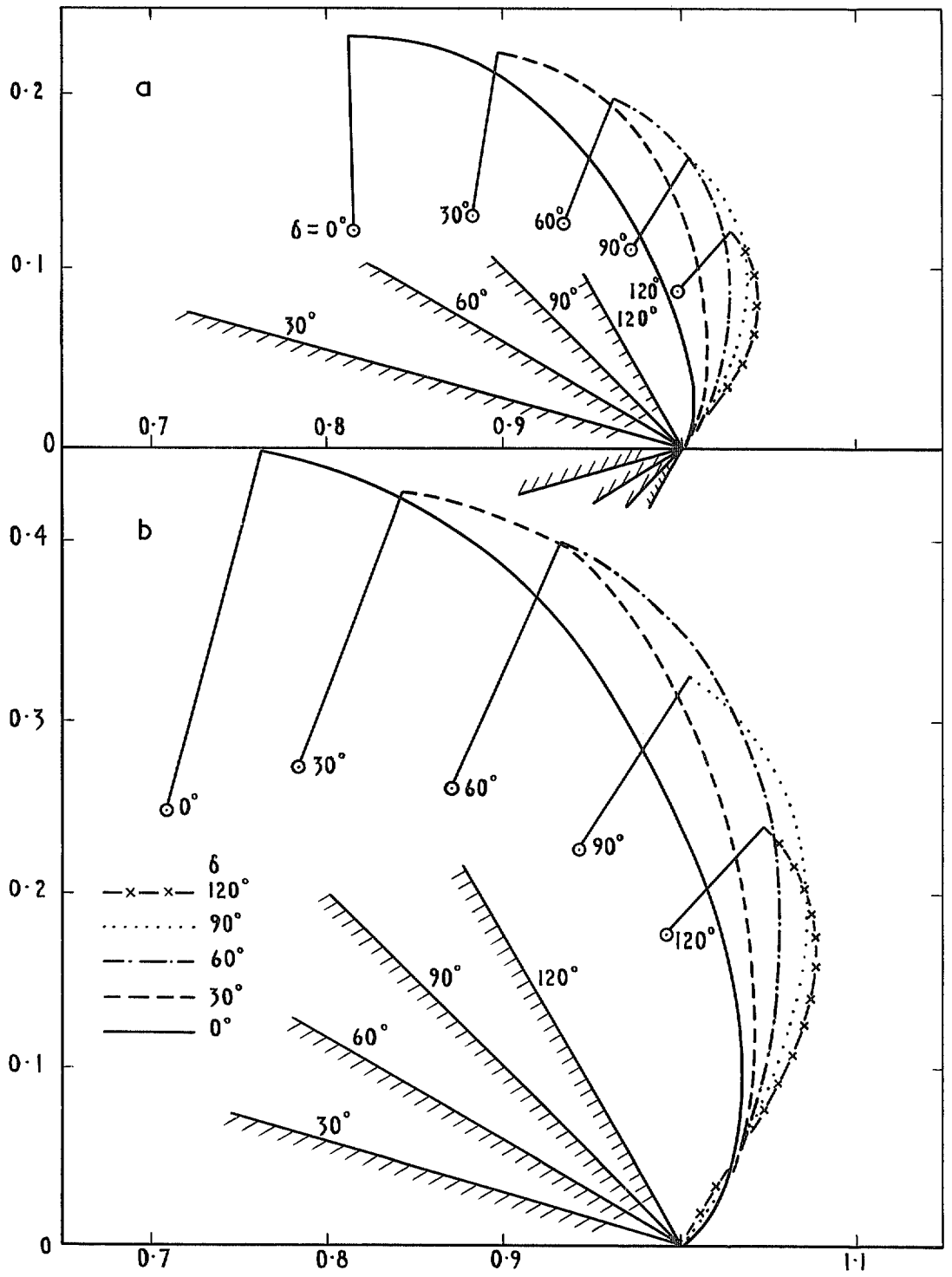

FIG. 8a & b. Variation of sheet shape and vortex position with thickness for $a = 0{\cdot}5$ and $1{\cdot}0$.

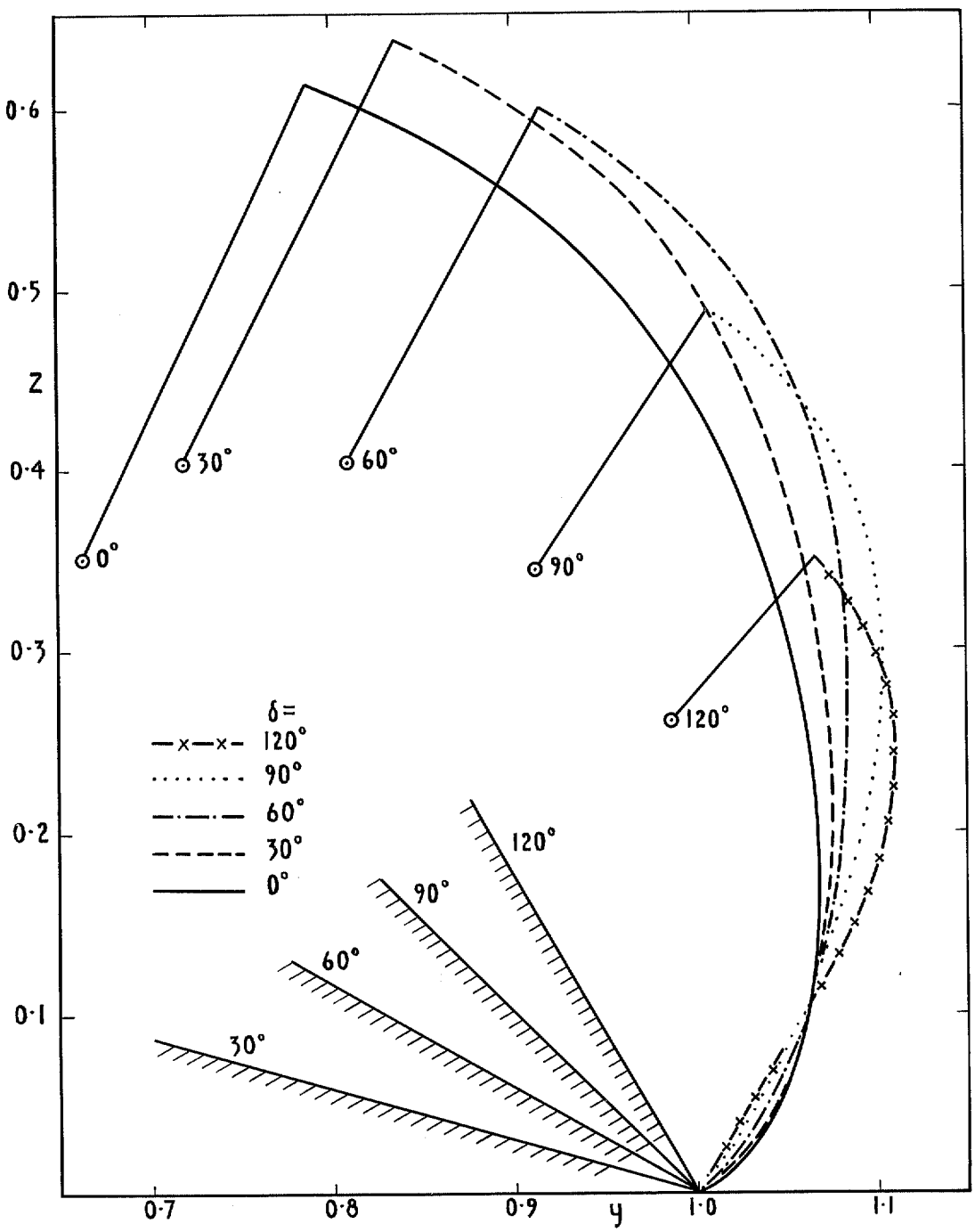

FIG. 8c. Variation of sheet shape and vortex position with thickness for $a = 1{\cdot}5$.

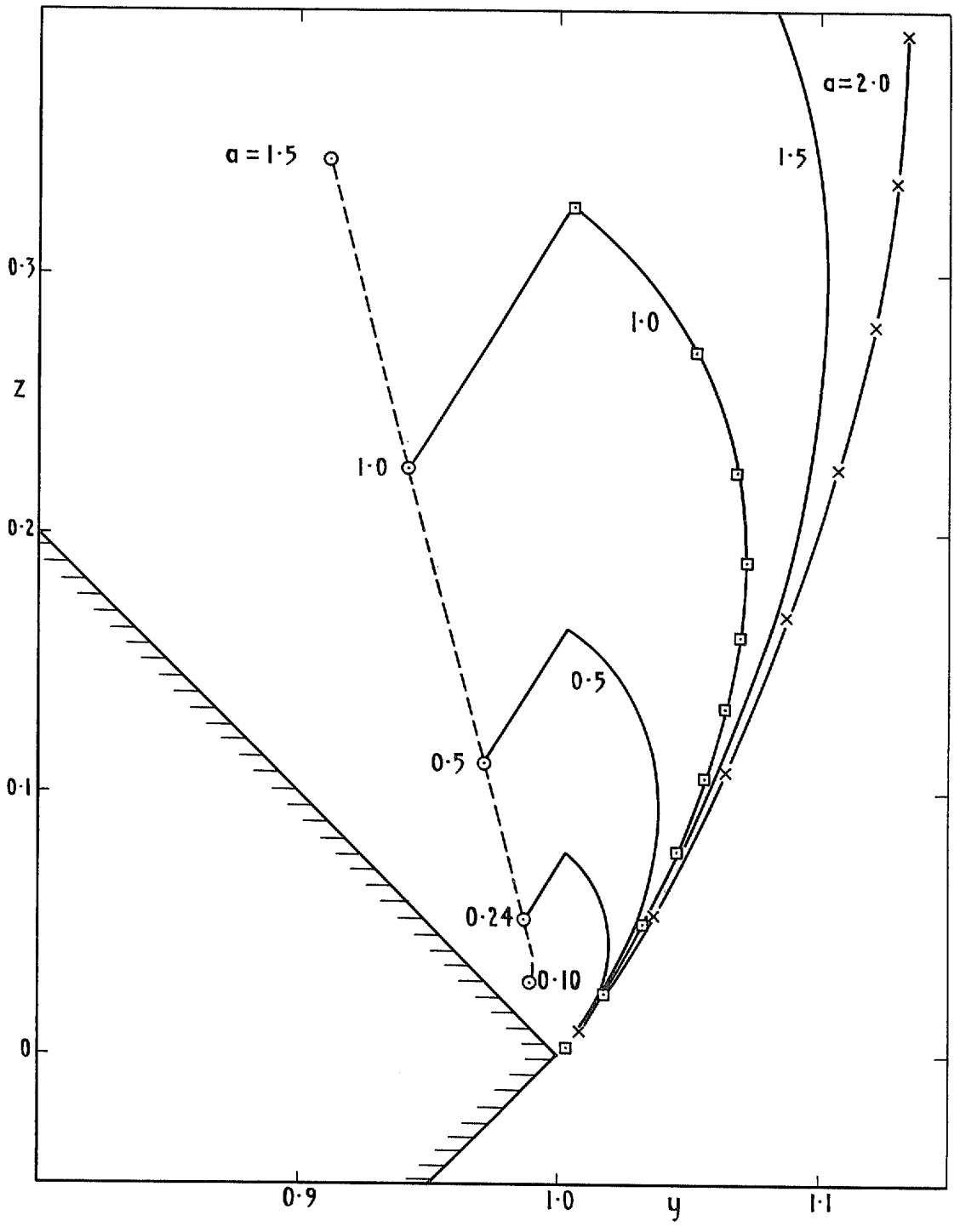

FIG. 9a. Variation of sheet shape and vortex position with a for $\delta = 90°$.

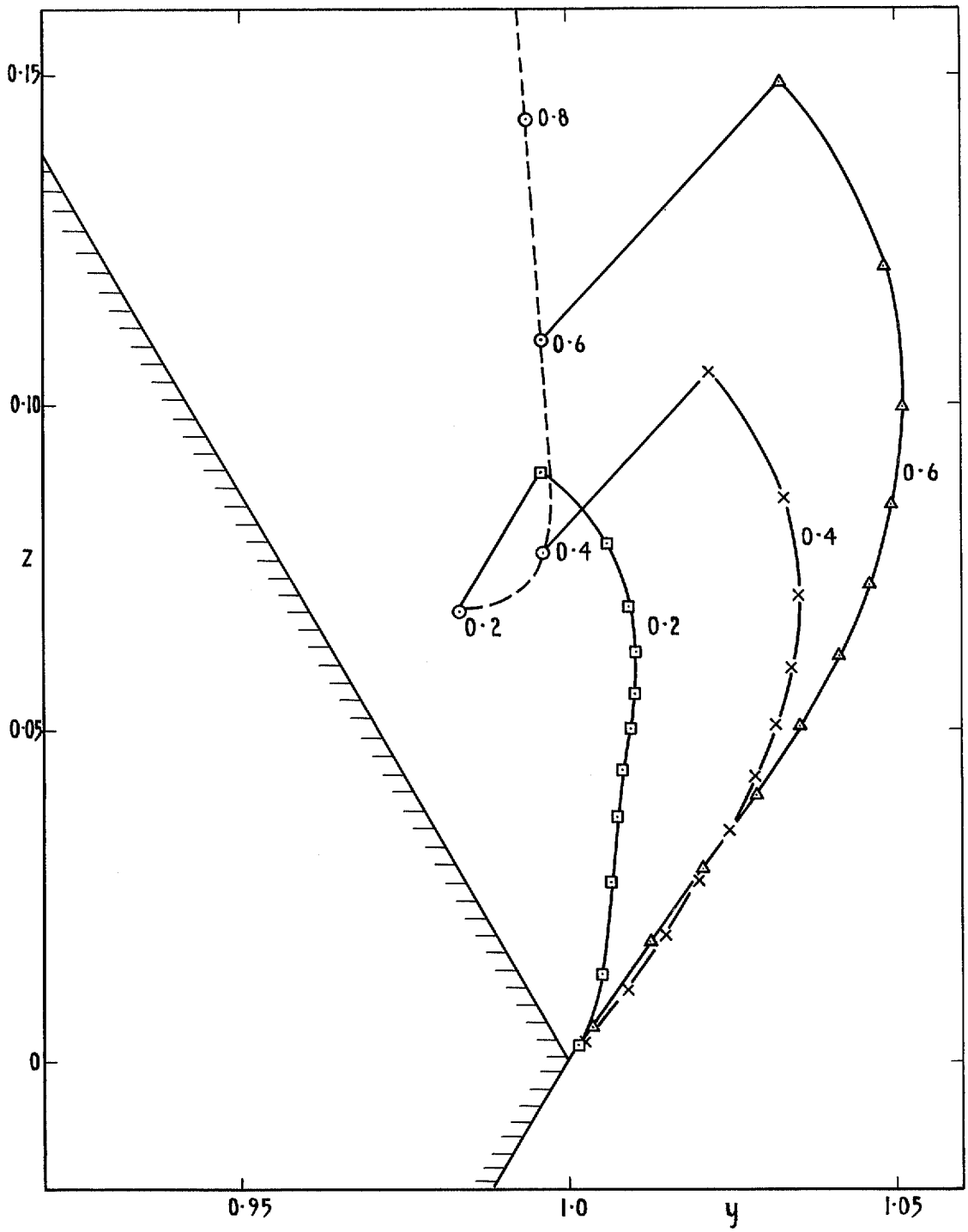

FIG. 9b. Variation of sheet shape and vortex position with a for $\delta = 120°$.

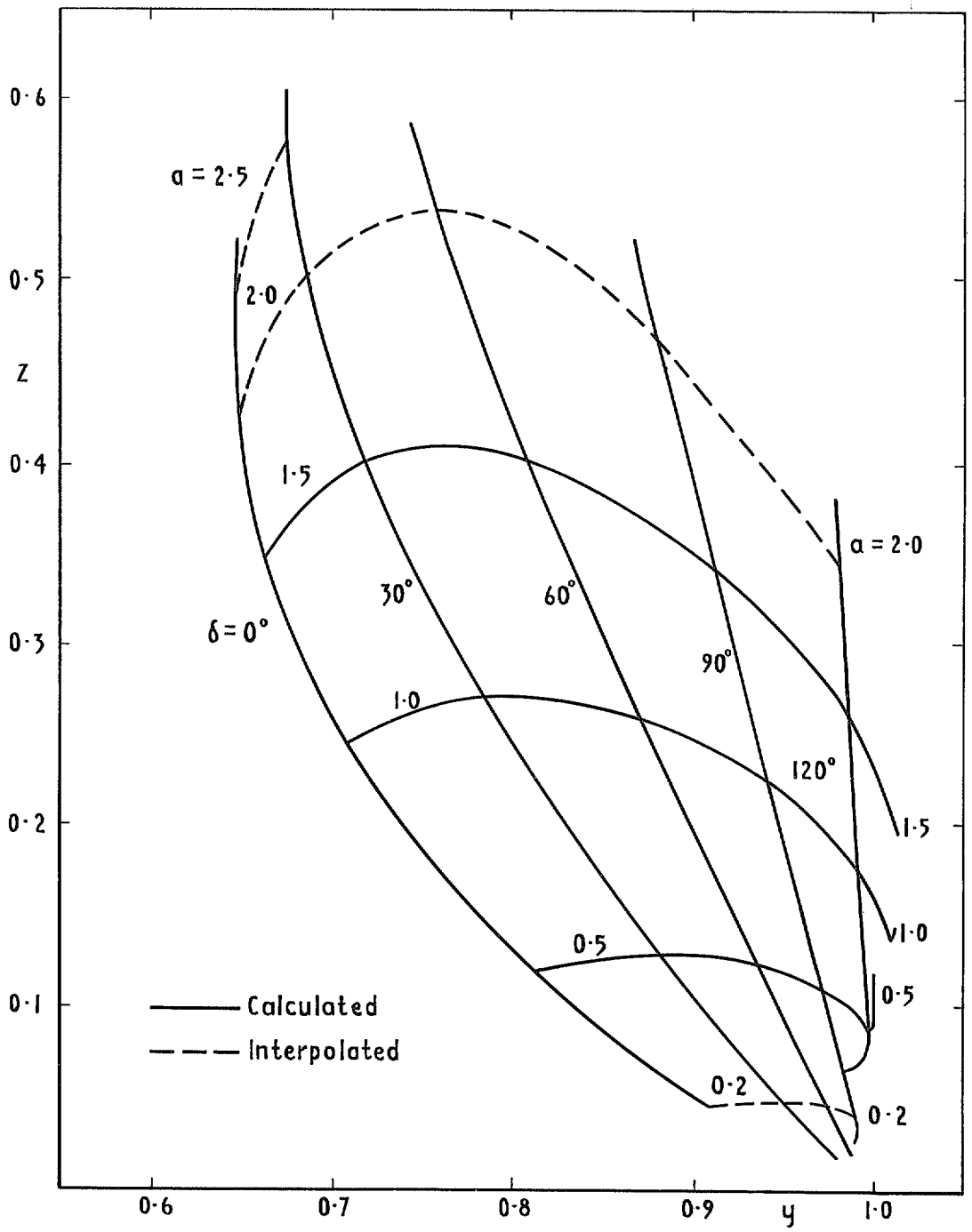

FIG. 10a. Calculated variation of isolated vortex position with thickness and incidence.

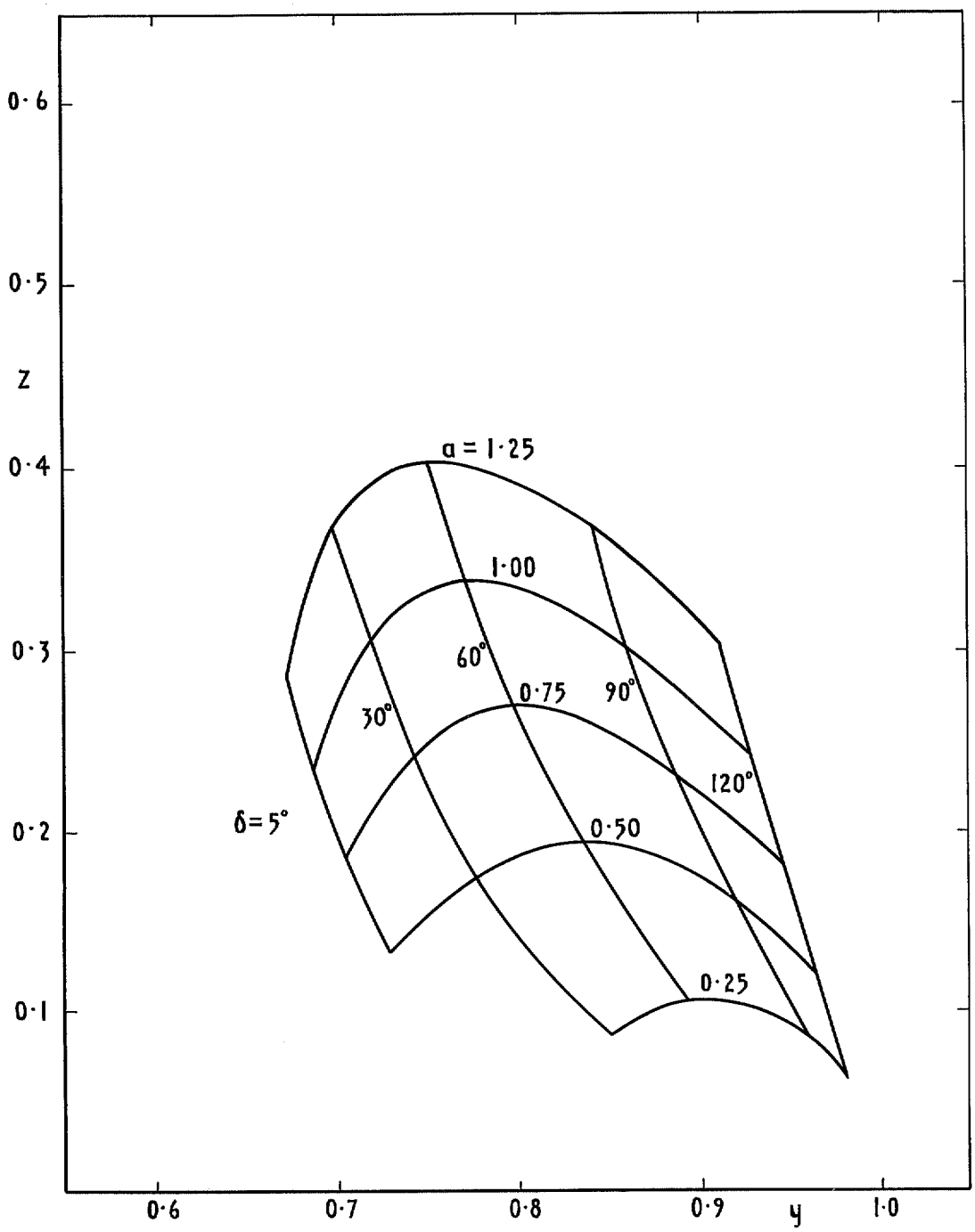

FIG. 10b. Measured variation of vortex centre with thickness and incidence (after Kirkpatrick & Field[19]).

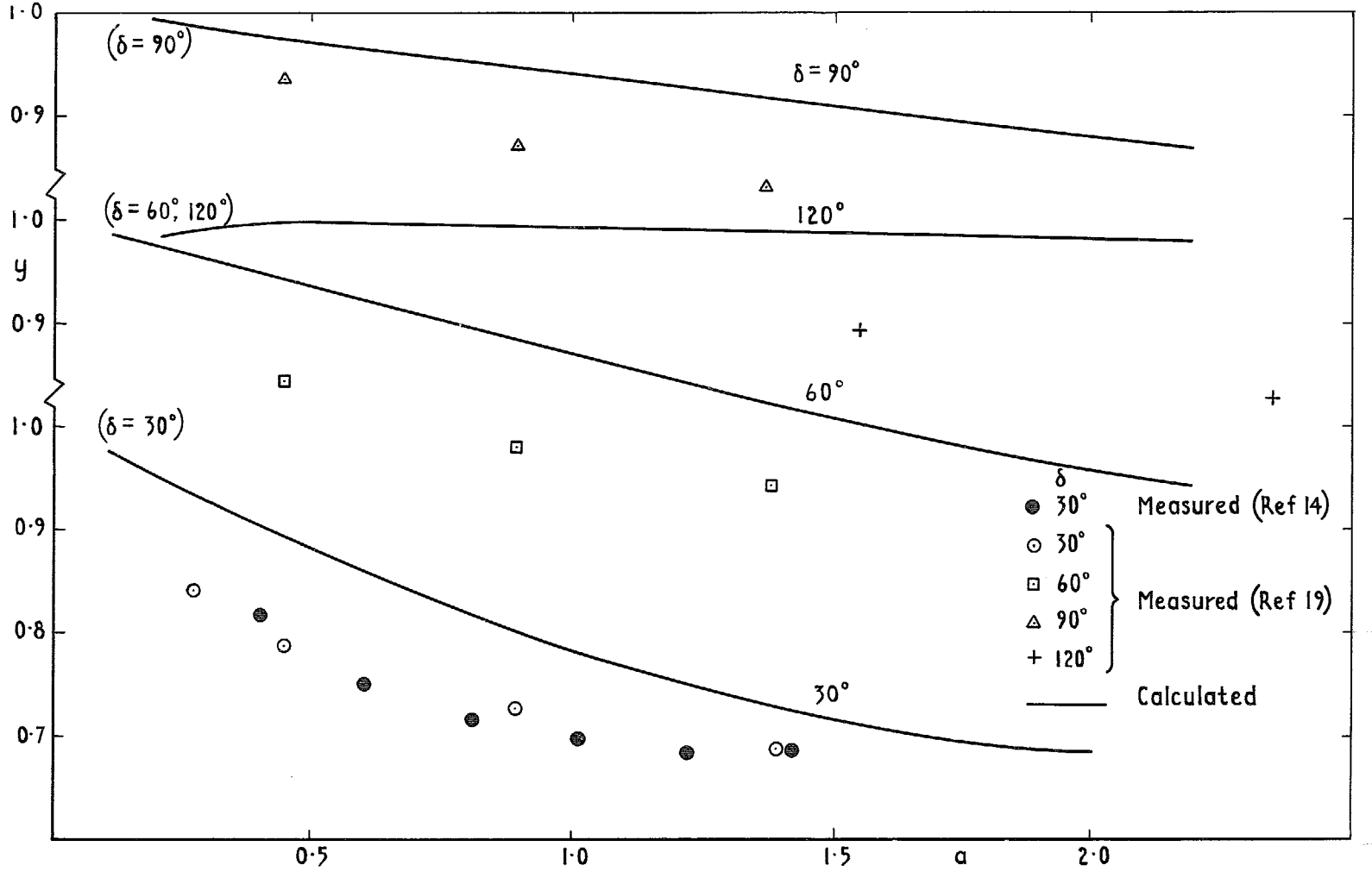

FIG. 11a. Lateral position of vortex: calculation and measurement.

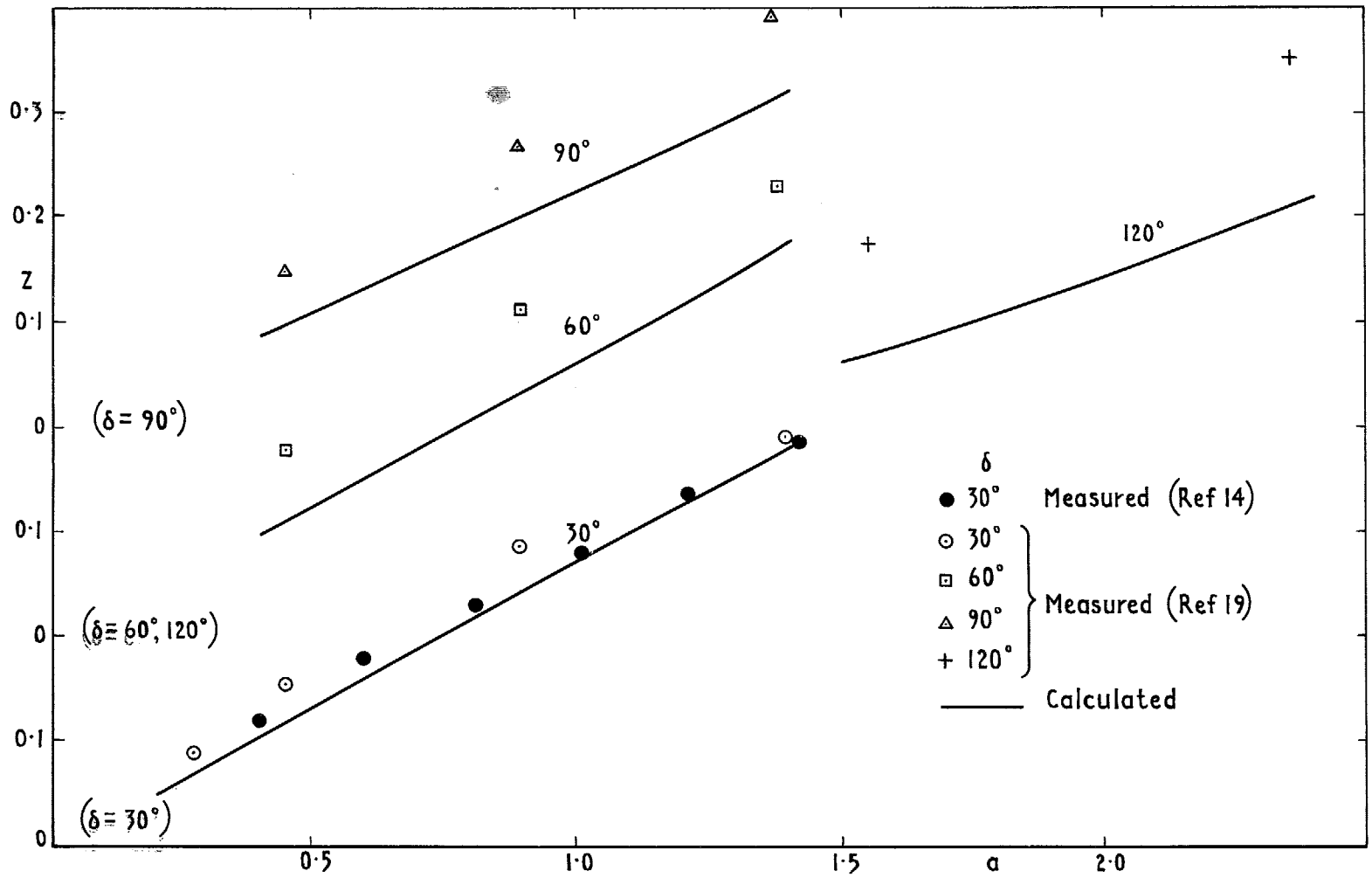

FIG. 11b. Height of vortex: calculation and measurement.

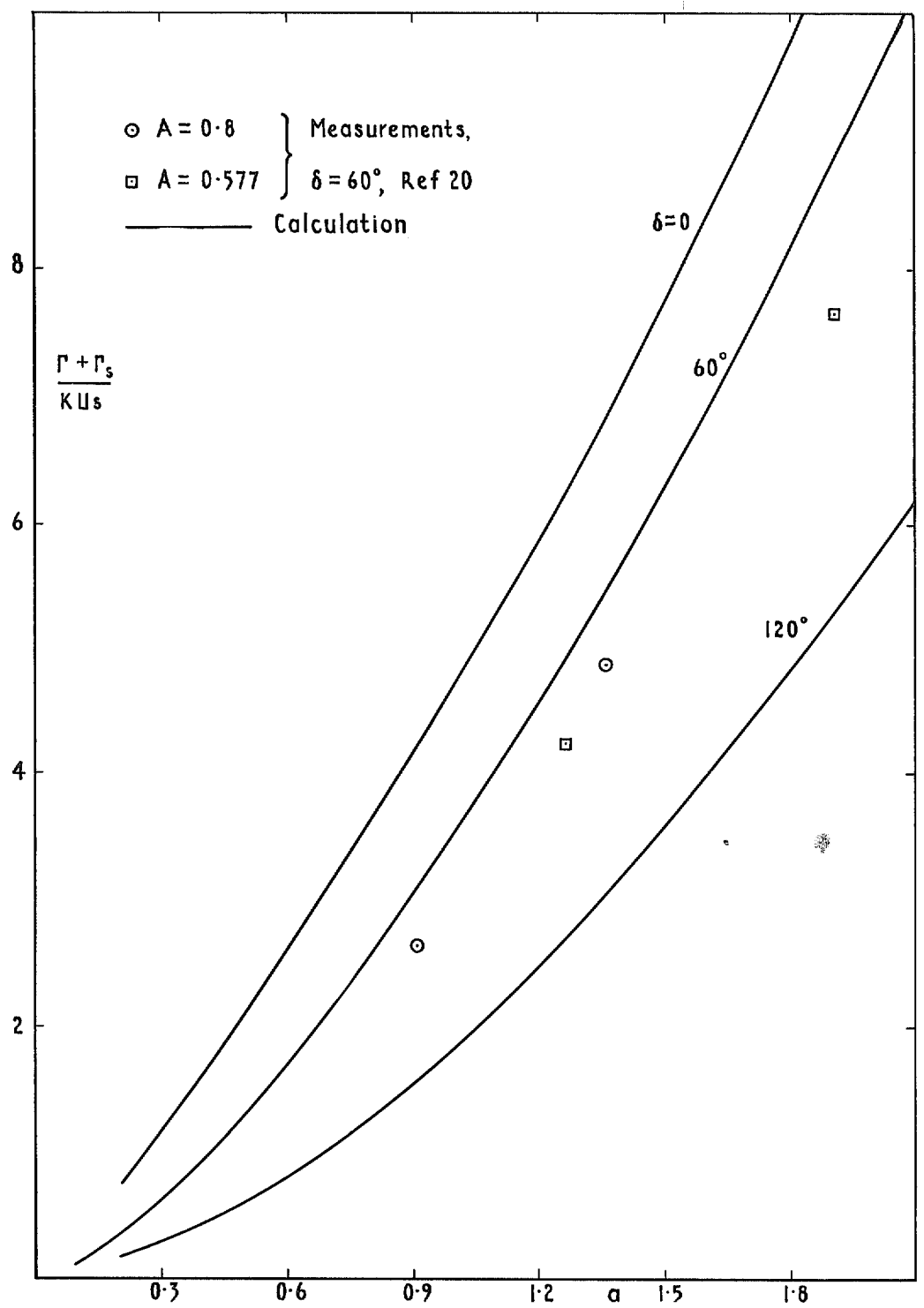

FIG. 12. Variation of total circulation with incidence.

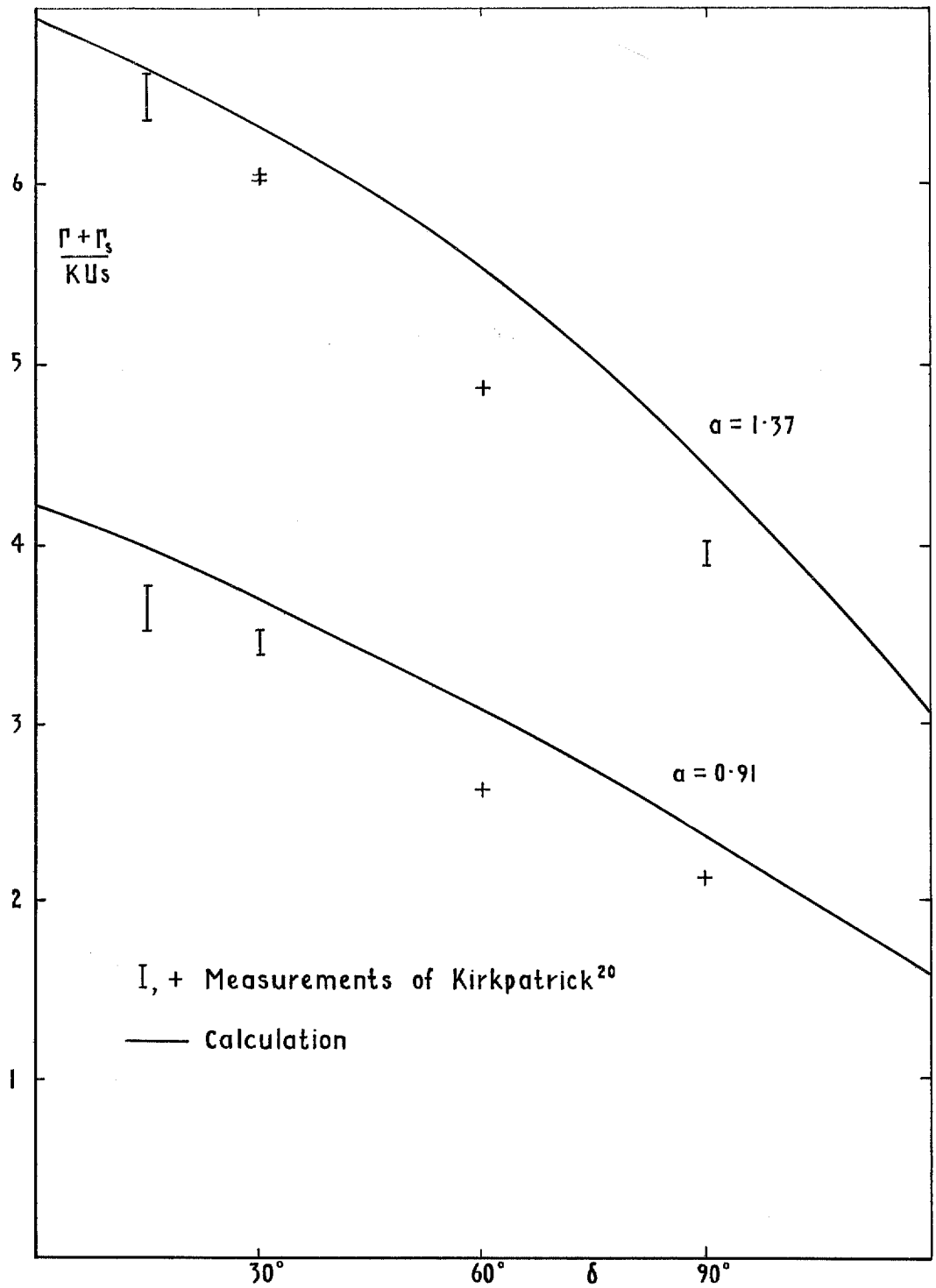

FIG. 13. Variation of total circulation with thickness.

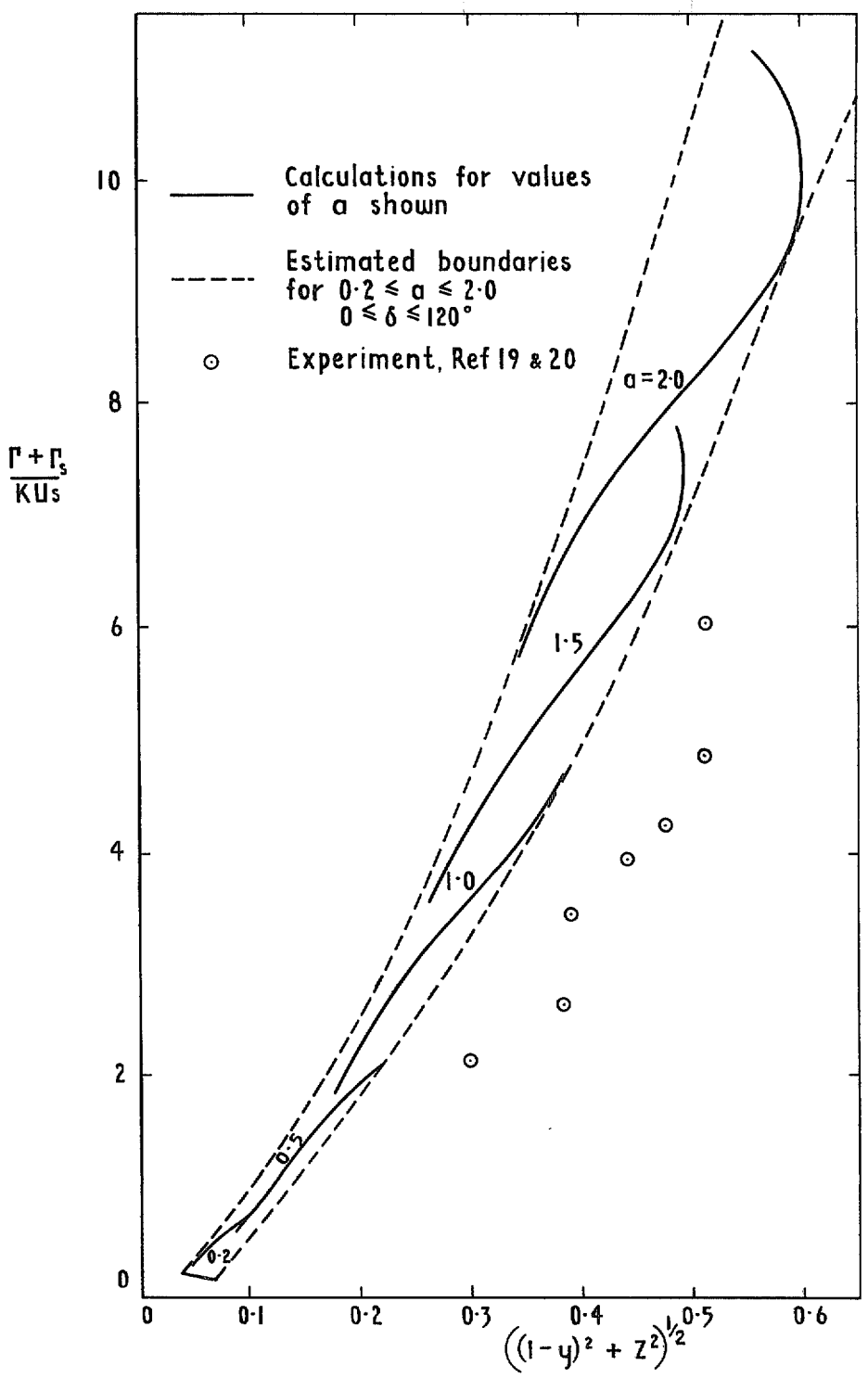

FIG. 14. Relation between scale and circulation of vortex.

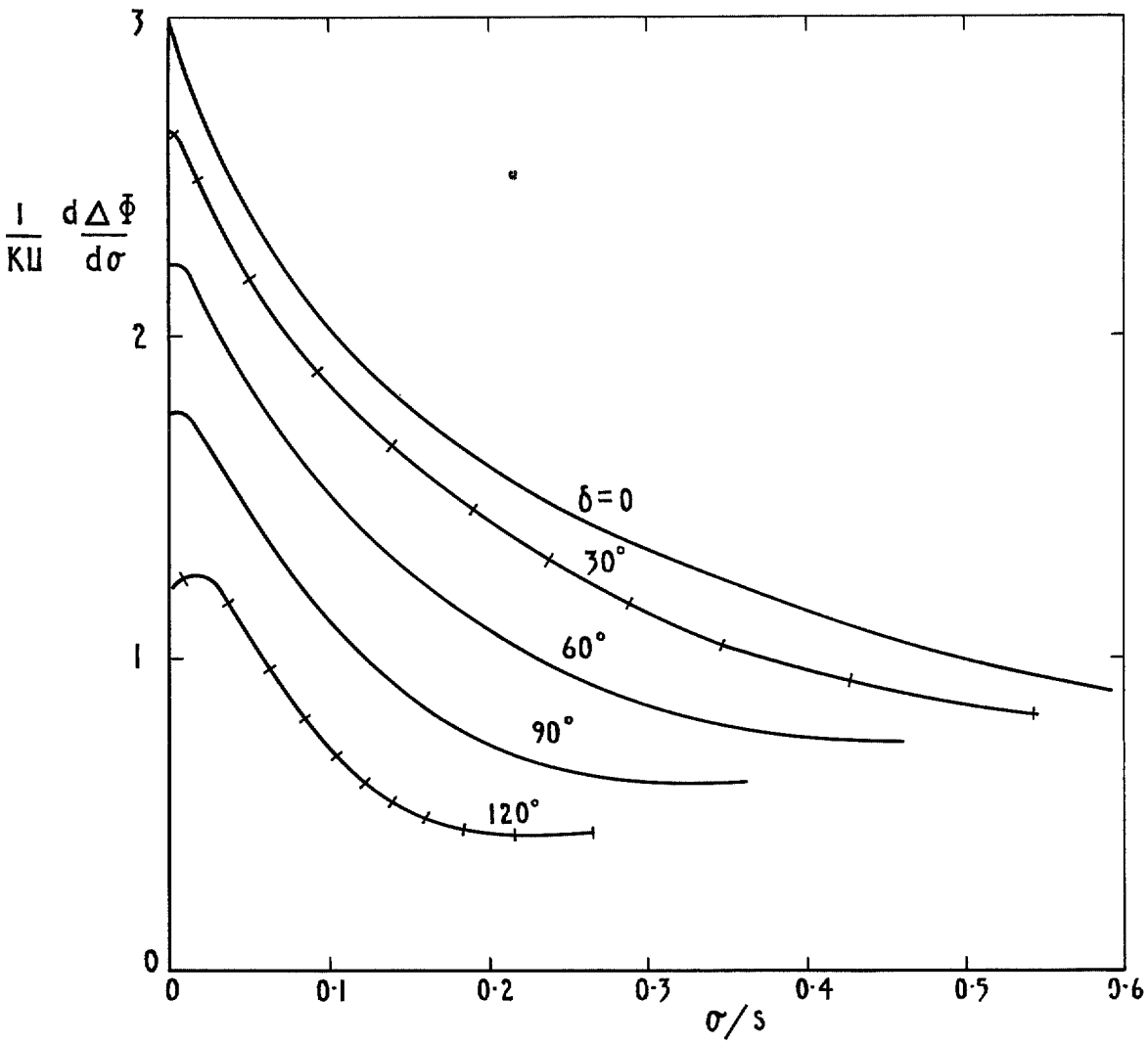

FIG. 15. Variation of sheet strength with thickness for $a=1$.

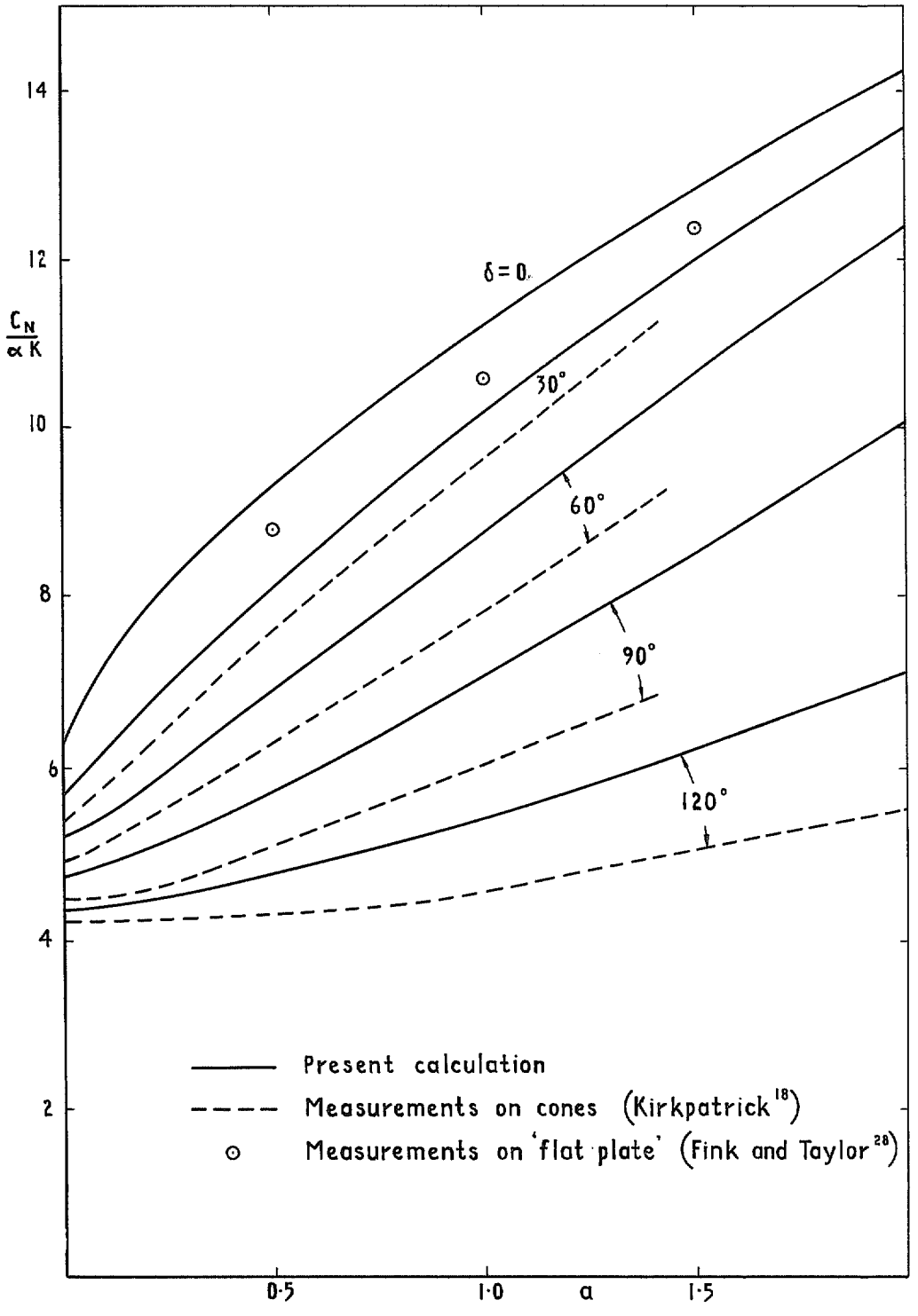

FIG. 16. Normal force in conical flow.

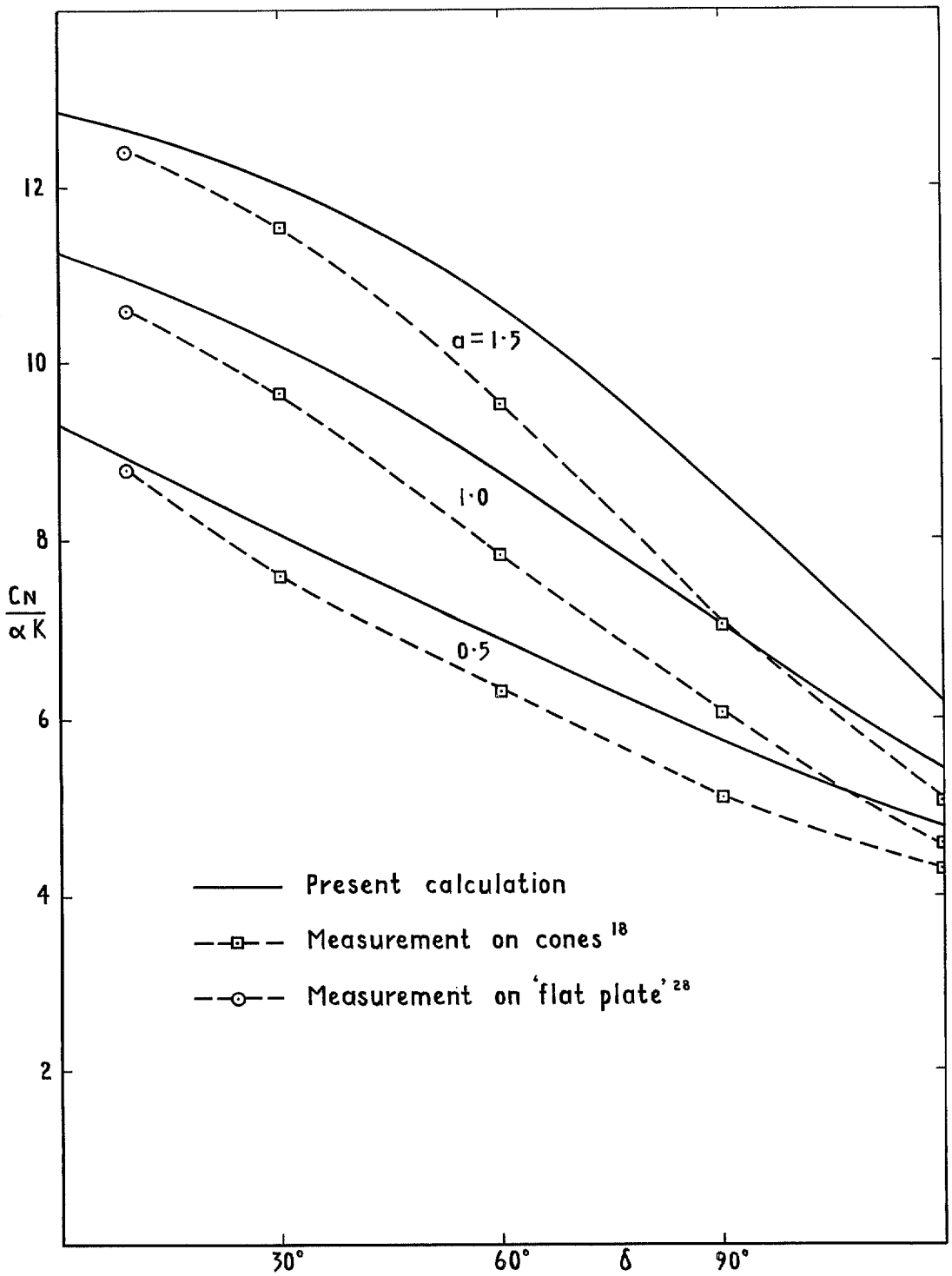

FIG. 17. Normal force in conical flow.

Printed in Wales for Her Majesty's Stationery Office by Allens Printers (Wales) Limited

Dd. 502110 K.5 2/72.

Published by
HER MAJESTY'S STATIONERY OFFICE

To be purchased from
49 High Holborn, London WC1V 6HB
13a Castle Street, Edinburgh EH2 3AR
109 St. Mary Street, Cardiff CF1 1JW
Brazennose Street, Manchester M60 8AS
50 Fairfax Street, Bristol BS1 3DE
258 Broad Street, Birmingham B1 2HE
80 Chichester Street, Belfast BT1 4JY
or through booksellers

R. & M. No. 3694
SBN 11 470494 5